The miR-96/RARγ signaling axis governs androgen signaling and PCa progression

Mark D Long[1], Prashant K Singh[2], James R Russell[1], Gerard Llimos[1a],

Spencer Rosario[1], Abbas Rizvi[3], Henry Withers[1], Patrick R. van den Berg[1b], Jason Kirk[4],

Lara E Sucheston-Campbell[3], Dominic J Smiraglia[1], Moray J Campbell[5]

[1]Department of Cancer Genetics, Roswell Park Cancer Institute, Buffalo, NY, 14263, USA

[2]Genomics Core Facility, Roswell Park Cancer Institute, Buffalo, NY, 14263, USA

[3]Division of Pharmacy Practice and Science, College of Pharmacy, 604 Riffe Building, The Ohio State University, Columbus, OH 43210

[4]Department of Pharmacology & Therapeutics, Roswell Park Cancer Institute, Buffalo, NY, 14263, USA

[5]Division of Pharmaceutics and Pharmaceutical Chemistry, College of Pharmacy, 536 Parks Hall, The Ohio State University, Columbus, OH 43210

[a]Current address Institute of Bioengineering, École Polytechnique Fédérale de Lausanne (EPFL), Lausanne, Switzerland.

[b]Current address: Leiden institute of Physics, Leiden University, 2300 RA Leiden, Netherlands

ABSTRACT

RARγ (*RARG*) expression is commonly reduced in prostate cancer (PCa). In prostate cell models reducing RARγ expression (*apo*), rather than retinoid ligand (*holo*) had the biggest impact on prostate cell proliferation and gene expression. The *apo* RARγ binds at active enhancers, enriched for AR, and regulates AR signaling. Testing RARγ capacity to govern AR, by knockdown, profoundly changed dihydroxytestostone capacity to regulate cell differentiation and gene regulation. RARγ regulated genes in TCGA PCa cohorts significantly associated with more aggressive disease. RARγ downregulation was explained by a stark and common increase in miR-96 in PCa cell and animal models, and human PCa. Biochemical approaches confirmed that miR-96 directly regulates *RARG* expression and function. Capture of the miR-96 targetome by biotin-miRNA pulldown identified a RARγ-centric network associated with more aggressive PCa and worse disease free survival. In summary, miR-96 targets an RARγ network to govern AR signaling and its disruption is a cancer-driver. Together, these findings support the concept that miR-96 governs the RARγ-network and prostate differentiation, in part by regulating AR. Tumors with high miR-96 and reduced RARγ-network expression significantly associated with poor disease free survival . These findings reveal how miRNA govern nuclear receptor cross-talk, and can be exploited to identify aggressive prostate cancer at an early stage.

INTRODUCTION

Members of the nuclear hormone receptor (NR) superfamily are ubiquitously expressed across tissues, and genomic approaches have revealed many examples of their integrated functions. Multiple NRs, including the androgen receptor (*AR/NR3C4*), are expressed in the normal prostate and their cross-talk is disrupted in PCa(1-6). For example, cross-talk occurs at the level of convergence on shared genomic binding regions, the sharing of co-factors and the co-regulation of ligand availability(7-10). More recently it has emerged that non-coding RNAs including miRNA and lncRNA target NRs, their co-factors and target genes to exert a further level of integrated control(11-16). Combined, these different aspects of NR regulation generate two signaling attributes, namely sensitivity and capacity; sensitivity is the magnitude of the transcriptional response, and capacity is the selection of gene networks governed.

One NR, the AR, is a key regulator of growth and differentiation in the prostate gland(17,18). Genomic approaches in prostate cancer (PCa) have identified that the capacity of the AR becomes skewed with disease progression(7,19-21). A normal component of AR signaling is to drive terminal differentiation of luminal epithelial cells and the phenotypic consequences of altering AR signaling capacity is, in part, to disrupt this function(22,23). The disruption, or re-wiring, of AR action changes both the sensitivity and capacity of AR and associates with PCa progression. Although the AR is a pharmacological target in later PCa stages(24), its disruption at early stage disease is more nuanced(25,26).

As a route to identify how NR networks in cancer are disrupted we undertook a pan-cancer analysis of the NR superfamily in The Cancer Genome Atlas (TCGA)(4,27). Application of bootstrapping approaches tested the significance of NR alterations, compared to 12 other transcription families(4,27-32), in various cancer types, including the Taylor et al MSKCC(33) and TCGA-PRAD PCa cohorts(34). This revealed a distinct NR profile within each tumor type suggesting that NR networks are disrupted in a tissue-specific manner(27) .

In PCa, the retinoic acid receptor gamma (*NR1B3*/*RARG*, encodes RARγ) (35) and glucocorticoid receptor (*NR3C1/GR*) were significantly and uniquely down-regulated in the MSKCC and TCGA-PRAD cohorts. By contrast, the AR was not significantly altered in either cohort. There was only one *RARG* mutation and relatively few CNVs detected at the *RARG* locus across these approximately 600 PCa samples.

Therefore we have examined the consequences and causes of reduced RARγ in prostate cells. We inspected the impact of reduced RARγ expression on cell phenotypes and gene expression,

both in the *apo* (non-ligand stimulated) and *holo* (ligand-stimulated) states, and revealed a substantial regulatory function specific to the *apo*-RARγ condition. Combined with analyses of the RARγ cistrome, these findings revealed that *apo*-RARγ significantly associates with gene enhancers, and impacts other TF functions including those of the AR. Testing how the RARγ governed the capacity and sensitivity of AR was undertaken by androgen-dependent transcriptomic analyses in cells with altered RARγ expression. Furthermore we revealed that miRNA-96, which is commonly elevated in PCa and associates with disease progression, is a key suppressor of the RARγ expression and a network of additional RARγ co-factors. Finally, across multiple PCa cohorts the miR-96 targetome and RARγ-dependent transcriptome associated with aggressive PCa and disease progression.

Together these findings support the innovative concepts that miR-96 regulates a RARγ centric network, which contributes a substantial portion of its function in the absence of retinoid activation as a major regulator of AR sensitivity and capacity, driving PCa progression.

RESULTS

Reduced RARγ expression promotes cell proliferation and widely alters gene expression in non-malignant and malignant prostate cell models.

To test if reduced RARγ levels are pro-tumorigenic, and to what extent retinoid responses are RARγ dependent, we knocked-down RARγ levels in non-malignant prostate epithelial cells (RWPE1) and LNCaP PCa cells using two separate RARγ targeting shRNA constructs (**Supplementary Figure 1A-F**). Remarkably, in RWPE1 and LNCaP cells in standard cell tissue culture conditions and without exogenous retinoids, RARγ knockdown increased growth rates within 72 hr (**Figure 1A**). By contrast, RARγ knockdown only modestly reduced anti-proliferative sensitivity in RWPE1 to either all-trans retinoic acid (ATRA) or RARγ-selective ligand, CD437 (**Supplementary Figure 2A-D**). Also, independent of exposure to ligand, RARγ knockdown significantly reduced the G_2/M population in both RWPE1 and LNCaP cells, whereas only in RWPE1 cells, reduced RARγ levels changed CD437-induced G_2/M blockade (**Supplementary Figure 2E-F**). Together these findings suggest that reducing RARγ expression has profound biological effects on growth and cell cycle control, which is largely independent of exogenous ligand.

Reducing RARγ levels exerted a significant impact on gene expression in the absence of ligand stimulation (*apo* function). The RARγ dependent CD437-induced response (*holo* function), defined as genes differentially regulated by CD437 in shCTL cells but not (or to a significantly lesser extent) in shRARG cells, was more modest (RWPE1) or negligible (LNCaP) (**Figure 1B-C**, **Supplementary Figure 3**). In RWPE1 cells, 605 differentially expressed genes (DEGs) (1.2 fold change, BH adjusted p-value < 0.05) were associated with *apo* RARγ regulation, whereas only 237 genes were responsive to CD437 (10 nM, 24 hr) in a RARγ dependent manner. The *apo* RARγ dependent transcriptome represented a near equal distribution of up- and down-regulated genes (338, 265 DEGs respectively). By contrast, the *holo* RARγ response was skewed consistent with the observation of ligand effects being predominantly transactivating (172, 52 DEGs respectively).

To infer functionality, Gene Set Enrichment Analysis (GSEA) was applied to the *apo* and *holo* RARγ dependent transcriptomes. 435 pathways were enriched (NES > 1.8, FDR q-val < 0.05) in at least one comparison (**Supplementary Figure 3F**). Amongst these, 196 were associated uniquely with *apo* function and 201 with *holo*, while 38 were common between categories. To reveal functional groupings commonly occurring within enriched gene sets in an unbiased

manner, title words from all gene sets were frequency mined to form meta-groups of common terms. To account for background frequencies of given terms across gene sets, hypergeometric testing was utilized to determine significant enrichment of meta-groups (**Figure 1D**). For instance, amongst all possible gene sets, 27 contained the term "NFKB" of which, 12 were significantly enriched for *apo* RARγ ($p = 6.46e^{-27}$). This approach revealed largely distinct functional annotations for the *apo* and *holo* RARγ states. For example, in RWPE1 cells *apo* transcriptome was significantly enriched for terms associated with NF-κB and histone deacetylase (HDAC) function (**Figure 1E**) whereas the *holo* transcriptome was enriched for terms related to Tretinoin (the commercial name for ATRA) (**Figure 1F**), as well as for ESR function. Similarly, in LNCaP cells, the *apo* RARγ gene regulatory effects were most pronounced (**Supplementary Figure 3C-D**) and highly enriched for hypoxia and AR responses (**Figure 1G, Supplementary Figure 3E-F**). Indeed, a previously compiled AR target gene panel (34,36) clearly distinguished LNCaP-shRARG cells from controls, in a CD437-independent manner (**Figure 1H**). Knockdown of RARγ in LNCaP also altered the DHT-induced expression changes in several key androgen target genes (i.e. *KLK3*, *TMPRSS2*) (**Supplementary Figure 3H**).

In total, these findings indicate that *apo* RARγ function is substantial and intertwined with other transcription factors, notably the AR and NF-κB, and functionally-independent of *holo* RAR function.

The *apo* RARγ cistrome significantly overlaps with active enhancers, AR cistromes and associates with aggressive PCa.

Next, we measured the *apo* and *holo* RARγ cistromes using RARγ-EGFP stably transfected in RWPE1 cells (37,38); optimization studies confirmed modestly-elevated RARγ-EGFP levels compared to endogenous RARγ, and enrichment at RARγ dependent genes (**Supplementary Figure 4A-C**). Reflecting the transcriptomic data, the *apo* RARγ cistrome was considerably larger (1256 peaks (p.adj < 0.1)) than the CD437-dependent cistrome of 360 peaks, of which 316 were shared, 44 were unique (**Figure 2A**). Motif analyses of the *apo* RARγ cistrome revealed significant enrichment of TF motifs from members of the AP1 family (FOSB/JUN), the homebox family (OTX2, PITX1) and NRs (RXRs, RARs). By contrast, and *holo* RARγ cistrome was enriched uniquely for CPEB1, ONEC2, HIC2 motifs as well as for FOSB/JUN (**Table 1**).

The RARγ cistrome was overlapped (within 100bp) with several RWPE1 data sets was investigated; DNAse sensitivity and histone modifications (H3K27ac, H3K27me3, H3K4me1,

H3K4me3)) (GSE63094, GSM1541008), and the ChromHMM chromatin states track for RWPE-1(39). Alongside these, normal prostate epithelial cell enhancers (40,41) and other cistromes derived in PCa cells were examined including AR, ERα and NF-κB-dependent cistromes(19) (**Figure 2B,C**).

The overlap of the *apo* RARγ cistrome with H3K27ac, H3K4me1 and DNAse sensitivity was striking; 829 RARγ binding sites overlapped with combined H3K27ac, H3K4me1 and DNAse sensitivity profiles. This suggests that the *apo* RARγ is very commonly found in open chromatin sites associated with active enhancer regions and was supported by the ChromHMM track. Significant overlaps were also identified between RARγ and both the *apo* and *holo* AR(42), and the DHT-dependent and TNF-stimulated p65 cistrome (19) (**Figure 2C**), supporting annotations revealed through transcriptomic approaches of RARγ function with AR and NF-κB functions (**Figure 1D**).

Next, we sought to dissect transcriptome-cistrome relationships. For example, *apo* RARγ strongly binds at the KRT15 locus in active enhancer sites, and its transcription is significantly altered by the knockdown of RARγ (**Figure 2D, E**). Both *apo* and *holo* RARγ cistromes were annotated to within 7.5 kb of known gene TSS. These cistrome proximal genes were then compared with genes found to be RARγ dependent from expression studies (**Table 2**). For example, the *apo* RARγ cistrome annotated to 512 unique genes, 159 of which were detectible at the expression level in the RWPE-1 microarray data. Bootstrapping tests were performed to examine if genes with proximal RARγ binding were more significantly regulated upon manipulation of RARγ status than the background transcriptome (**Figure 2F**). The results demonstrate that both the apo and holo RARg cistromes are significantly associated with genes whose expression changes upon loss of RARg, supporting a functional relationship between binding and expression control

In the TCGA-PRAD and MSKCC cohorts the RARγ-annotated genes more positively correlated with RARγ than predicted by chance **(Supplementary Figure 5A,B)** and filtering these RARγ cistrome genes (altered by greater than 2 Z scores in more 35% tumors relative to normal tissue) identified 58 genes. Expression of these genes stratified patients (**Figure 2G**) and distinguished a cluster of high Gleason grade tumors (adjusting for age) (Pearson's Chi-squared test X-squared = 51.187, df = 35, p-value = 0.038). Individually, approximately 20% of these genes (12) associated with worse disease free survival, for example including the steroidogenic enzyme *CYP11A1*(43) (**Figure 2H**). Other genes significantly associating with disease free

survival are *LRG6*, which is a WNT regulator and implicated in breast cancer(44); *PRR7*, which is a central regulator of CLOCK; *GPX3* which is a negative regulator of prostate growth(45); *PDLIM4* which is aberrantly methylated in PCa downstream of MYC and RAR signaling and suppresses PCa(46).

Reduced RARγ expression alters AR signaling capacity and sensitivity.

The cellular phenotype, transcriptome and cistrome data support the concept that *apo* RARγ actions represent a substantial portion of all RARγ genomic functions and are intertwined with other TFs including the AR. Therefore, we sought to test the genome-wide impact of RARγ expression on AR function directly in non-malignant prostate epithelial HPr1AR cells. These cells constitutively express AR, and undergo androgen-induced differentiation from a basal-like towards a more luminal-like phenotype (47,48). RARγ knockdown reduced RARγ levels 60-80%, which was not altered by DHT (**Supplementary Figure 6A-D**).

The anti-proliferative response induced by DHT was significantly dampened in RARγ knockdown HPr1AR cells (**Figure 3A**), suggesting *apo* RARγ function impacts AR signaling capacity and/or sensitivity. This concept was also supported globally at the transcriptome level (RNA-Seq), which revealed that RARγ knockdown substantially reduced DHT-dependent transcriptome changes at both 24 and 96 hr (**Figure 3B-C, Supplementary Figure 7A-B**). For example at 24 hr, 1454 of the 2309 (63.0%) DHT-regulated DEGs were either no longer regulated or had significantly dampened regulation in RARγ knockdown HPr1AR cells. The sensitivity switch in response to RARγ loss was directional, as all DHT-responses were dampened rather than amplified. However, the capacity of DHT regulation was also shifted, albeit to a lesser extent, as a small number of genes (109) gained unique DHT-regulation following RARγ knockdown in HPr1AR cells at 24 hr. Thus, RARγ knockdown substantially impacted both the sensitivity and the capacity of the AR-regulated transcriptome.

GSEA identified enrichment for androgen response pathways (**Figure 3D-F**), as well as MYC and hypoxia associated pathways (48), consistent with a shift towards luminal differentiation and an anti-proliferative response to DHT. In line with observations at the gene level, the extent of pathway regulation by DHT was significantly reduced in RARγ knockdown HPr1AR cells. For example, classic androgen response pathways were not elevated to the same extent in RARγ knockdown cells relative to parental HPr1AR cells, and conversely the repression of MYC regulated pathways was less apparent. Notably, a prominent RARγ binding peak was identified in an enhancer region upstream of MYC (**Supplementary Figure 7D**).

Together, this suggest that independently of exogenous retinoid ligand RARγ expression governs AR function in normal prostate cells, with its loss dampening both phenotypic and transcriptomic androgen responses, which manifest as reduced luminal differentiation and reduced antiproliferative signaling.

Elevated miR-96 drives reduced RARγ expression and associates with aggressive prostate cancer.

The frequent downregulation of *RARG* reflected neither mutation nor copy number variation(27) and therefore we considered epigenetic mechanisms, but found no evidence for altered DNA methylation in the TCGA-PRAD cohort (**Supplementary Figure 8**). Therefore, we considered miRNA, and used *in silico* prediction tools(49) to define a cohort of miRNAs that target the most common previously identified downregulated NRs (i.e. *RARG, GR*) in the TCGA-PRAD and MSKCC cohorts (27).

Specifically, 61 putative NR-targeting miRNAs were identified (**Supplementary Figure 9**) and bootstrapping approaches revealed these miRNA were collectively more elevated in PCa samples than predicted by chance (p.adj = 0.02) and were reciprocal to the reduction of NR mRNA expression. The miR-96-182-183 cluster was amongst the most commonly upregulated miRNAs. Although similar, base substitutions in the targeting regions of each miRNA suggest unique functionality (**Supplementary Figure 10A**). Only miR-96 and miR-182 have predicted target sequences in the *RARG* 3'UTR (**Supplementary Figure 10B**).

In both the MSKCC and PRAD cohorts, *RARG* significantly and negatively correlated with cluster members, but most strongly with miR-96 (**Figure 4A**). Expression analyses in a panel of prostate cell lines (**Figure 4B**) revealed miR-96 increases relative to non-malignant RWPE1 and HPr1AR cells, in six PCa cell lines and reduction in *RARG* expression. Profiling in PCa mouse models revealed reduced *Rarg* in both Pten$^{-/-}$(50) and to a greater extent in TRAMP(51) but, interestingly, not in Hi-MYC(52) mice (**Supplementary Figure 11A**). *Rarg* expression decreased dynamically with PCa development in TRAMP mice, relative to age-matched wild-type controls (C57BL/6), and inversely correlated most significantly with elevated miR-96 expression (Pearson's r = -0.88) (**Figure 4C**, **Supplementary Figure 11B**). Notably, significant expression changes were observed as early as 10 weeks of age, when TRAMP mice display prostate epithelial hyperplasia. Finally, relative expression changes of *RARG* and miR-96 cluster members in human PCa were validated in an independent cohort of 36 matching tumor/normal tissue pairs and significantly associated with Gleason sum (**Supplementary Figure 12A-C**), corroborating observations in TCGA-PRAD and MSKCC cohorts. Additionally

miR-96 expression in the TCGA-PRAD cohort stratified patients based on shorter disease free survival (**Supplementary Figure 12D**). Together these findings in mice and humans suggest that increased miR-96 expression is an early and continuous event in PCa development, correlates strongly with loss of *RARG* and associates with aggressive disease subtypes.

Two miR-96 recognition elements were identified in the *RARG* 3'UTR region (**Supplementary Figure 10B**). Ectopic overexpression of miR-96 resulted in significant loss of RARγ mRNA and protein in both RWPE1 and LNCaP cells (**Figure 4D, Supplementary Figure 13A-C**) and co-transfection of a *RARG* 3'UTR luciferase vector with a miR-96 mimic resulted in significant loss of luciferase activity (**Figure 4E**). Finally, miR-96 suppressed RARγ ligand-dependent induction and repression of target genes, which was alleviated by a miR-96 antagomiR (**Figure 4F**).

Lastly, transfection with miR-96 mimics led to a marked increase of proliferation in LNCaP cells, reflecting phenotypes observed in RARγ knockdown cells (**Figure 1**). Exogenous miR-96 also altered the cell-cycle distribution. For example in LNCaP cells there was a loss of cells in G_1/G_0 phase (53.2% relative to 64.8%) and increase in S and G_2/M phase (**Figure 4G** and **Supplementary Figure 14**). However, cell cycle shifts in LNCaP did not mirror those observed in RARγ knockdown cells, and no significant changes were noted in RWPE1 cells, suggesting that miR-96 related phenotypes involve additional targets other than RARγ.

Together, these findings support the concept that elevated miR-96 targets and suppresses *RARG* expression and function, an interaction which occurs early in PCa progression and which has pro-tumorigenic properties.

MiR-96 targets a network of RARγ interacting co-factors.

While these data strongly support miR-96 targeting of RARγ, other studies have identified additional targets, including the pioneer factor FOXO1(53-55), which have biological consequence in prostate cells. Therefore, to reveal all miR-96 targets (the miR-96 targetome), we undertook a biotin-miRNA (bi-miR) pulldown approach coupled with microarray analyses(56). Biotin labelling of miR-96 mimics did not interfere with either transfection or knockdown of target gene expression (**Supplementary Figure 15A-B**), and was able to capture known (e.g. *RARG* and *FOXO1*) and predicted (*TBL1X*) miR-96 targets (**Supplementary Figure 15C**). PCA revealed strong separation of experimental groups (**Supplementary Figure 15D**).

The bi-miR-96 pulldown revealed 111 and 389 miR-96 targets in RWPE1 and LNCaP cells, respectively, which were largely shared, but also had unique genes (**Figure 5A-B**

Supplementary Figure 15E). Amongst these targets, 3'UTR miR-96 target site motifs (GTGCCAA) was the most highly enriched (**Figure 5C**) (GSEA in LNCaP p.adj = $1.24e10^{-26}$, RWPE1 p.adj = $1.70e10^{-9}$). RT-qPCR validation of independent LNCaP cells confirmed the direct binding of miR-96 to known and novel targets identified from profiling (**Supplementary Figure 15F**).

Interestingly, in LNCaP cells *FOXO1* was neither significantly enriched in the bi-miR-96 fraction upon microarray analysis and was only validated by RT-qPCR in RWPE1 cells. Also surprisingly, *RARG* transcript was not significantly detectable via microarray in either LNCaP or RWPE1 cells, but did validate by RT-qPCR in both cell types. It was revealed that the Illumina HT12v4 Bead Chip array contains only a single exon probe targeting a single *RARG* isoform. *RARG* expression in LNCaP cells has been reported by us(6) and others(57) suggesting that the microarray finding is a false negative one.

The capacity of miR-96 to suppress target gene expression was also assessed by independent transfections of biotinylated and non-biotinylated miR-96 mimics. In LNCaP cells, 6 out of 7 bi-miR-96 identified targets were significantly downregulated by both miR-96 and bi-miR-96 relative to respective non-targeting controls, while a negative control target *CDH1* was not affected (**Figure 5D**). Intriguingly, the single transcript not downregulated in this experiment, p27 (encoded by *CDKN1B*), showed significantly reduced protein level upon miR-96 overexpression, suggesting that in some cases the result of miR-96 binding is translational inhibition not degradation of transcript (**Supplementary Figure 15G, H**).

Functional annotation of the miR-96 targetome in LNCaP cells based on GO terms revealed roles for miR-96 in governing cell cycle progression, metabolism, cell morphology and microtubule organization (**Supplementary Figure 16A,B**). These observations reflected the impact of miR-96 on cell cycle and included *CDKN1B*, *CDK2*, *DICER1* and transforming acidic coiled-coil protein 1 (*TACC1*). The top five most significant inverse miR-96/mRNA relationships included cell-cycle regulators and transcription factors. Expression after miR-96 overexpression in LNCaP cells revealed several were significantly suppressed (**Supplementary Figure 16C,D**).

To assess whether experimentally determined targets had relationships in clinical samples, TCGA-PRAD data were again examined. Genes within the miR-96 targetome showed a significantly more negative correlation with miR-96 expression than the background transcriptome, supporting a functional relationship (K-S test p = $5.17e^{-7}$) (**Figure 5E**). Stringent filtering of expression of the miR-96 targetome genes (+/-2 Z scores in 35% of tumors relative to normal prostate tissue) identified 22 altered genes that modestly, but significantly, that

segregated invasive tumors, after adjusting for age at diagnosis (Pathological N1; X-squared = 89.539, df = 68, p-value = 0.041) (**Figure 5F**). Five of these 22 genes were known to regulate RAR signaling (i.e. TACC1(58), ZIC2(59), PRKAR1A(60), EIF4G2(61), YAP1(62)), and ONECUT2 is a putative co-regulator (63), the motif for which was enriched in the experimentally derived *holo* RARγ cistrome. Also, expression of five of the 22 genes individually associated with worse disease free survival including ZIC2 and TACC1 (**Figure 5G**).

The miR-96 governed RARγ network drives aggressive prostate cancer.

Several lines of evidence support the concept that miR-96/RARγ is a significant signaling axis in the prostate; the levels alone of *apo* RARγ control gene expression and govern AR function; miR-96 governs the levels of *apo* RARγ and a number of interacting co-factors; the expression of miR-96 and RARγ are reciprocal in murine and human tumors; RARγ targets and miR-96 targets predict aggressive PCa tumors.

We next sought to establish the combined significance of miR-96/RARγ axis in PCa. We segregated tumors in the TCGA-PRAD cohort into low expression of both RARγ and TACC1 (as they strongly correlate) and high miR-96 expression, compared to the reciprocal (high RARγ and TACC1, low miR-96) (**Figure 6A**). Differential expression identified ~1700 genes, which were in turn overlapped with the gene sets developed through the study. Several of the overlaps support the concept of a miR-96/RARγ axis. For example nearly 200 genes were shared between the *apo* RARγ-dependent gene expression and the DHT-regulated and shRNA RARγ-dependent genes, and 31 of these significantly overlapped (p=7.1e-6) with the genes identified in TCGA-PRAD (**Figure 6A**).

We reasoned that if genes central to the miR-96/RARγ axis were critical in PCa, they would be commonly distorted and associate with aggressive disease. Filtering the ~1700 differentially expressed genes in RARγ low/miR-96 high tumors (altered by +/-2 Z scores in more than 45% of tumors relative to normal prostate tissue) revealed 47 genes that separated those with significantly worse disease free survival (X_REFS_IND) in the TCGA-PRAD cohort (logrank test p-val = 0.026) and also clustered high Gleason score tumors (X-squared p-val = 0.012) (**Figure 6B**). Genes were also annotated for whether they were an *apo* RARγ cistrome gene; DHT-regulated RARγ-dependent genes; member of the highest rank GSEA term was (LIU_PROSTATE_CANCER_DN; a cohort of genes significantly down-regulated in PCa(64)) as well with survival outcomes. For example, SOX15 was a shared *apo* RARγ cistrome gene and DHT-regulated RARγ-dependent gene (**Figure 6C**) and loss of expression of PPARGC1A and

ACOX2 both were associated with worse disease free survival (**Figure 6D**). These findings support the concept that the miR-96/RARγ axis can be detected in PCa cohorts, further underscores its cross talk with AR signaling and its clinical relevance.

DISCUSSION

Developmental roles for RARγ have been identified in skin, skeletal and reproductive systems, including the prostate (65). Prostate epithelial squamous metaplasia arises in *Rarg-/-* mice, due to improper glandular function (65). More broadly, RARγ has emerged as an important transcription factor. For example, the Roadmap Epigenome consortium identified RARγ as a member of the most highly enriched in transcription factor-enhancer interactions across the human epigenome(66) and others have considered a role for the receptor to govern pluripotency(67). *RARG* has also been suggested to be a tumor suppressor in keratinocytes(68). Previously, we identified a common RARγ down-regulation in the TCGA-PRAD and MSKCC cohorts.

We have now identified that the *apo* actions of RARγ are substantial, and more significant than the impact of retinoid exposure as seen with our microarray and ChIP studies, but also our analyses of microarray studies in RAR$\gamma^{-/-}$ murine ES cells and also F9 cells, (69,70) where similar patterns were observed (**Supplementary Figure 17)**. These findings are also compatible with other receptors such as RARβ being more prominent in the sensing of exogenous ligand in PCa cells (6,71).

The current study also revealed RARγ regulation of AR signaling in PCa. The *apo* RARγ transcriptomic studies revealed enrichment of AR signaling processes, notably in LNCaP, whereas in RWPE1 cells the transcriptome was enriched for ESR function, further supporting RARγ functional crosstalk with steroid receptor signaling. Links between RARs and ER signaling which are well established in breast cancer(37).

Genomic *apo* RARγ binding very significantly overlapped with active enhancers (RWPE-1) and AR binding (LNCaP), and also significantly regulated the DHT-AR transcriptome in HPr-1AR cells. RARγ loss profoundly altered AR regulated events including DHT-mediated anti-proliferative effects (48) and reduced the DHT-dependent transcriptome, notably by restricting the capacity of AR to repress MYC signaling. Recently MYC has been shown to antagonize AR function in prostate cells(72), and the current study suggest that RARγ regulates these events, in part through direct binding at the MYC locus. Together these findings supported the concepts that the *apo* RARγ is significantly associated with enhancers, and governing AR functions.

Although miR-34c targets *RARG* in embryonic stem cells(73), we found no significant relationship between miR-34c and RARγ in the current study. Rather we identified miR-96, which has been investigated in various cancer settings including in PCa, but not associated with

RARγ (53-55,74-77). Furthermore, miR-96 is one of the 60 miRNAs whose expression most differentiated PCa clinical groups in TCGA-PRAD cohort(78). The current study extends these reports of oncogenic actions of miR-96 to identify the RARγ network as a major biological and clinically-relevant target.

The inverse relationships between miR-96 and RARγ was robust and significant across cell models, murine PCa models and clinical cohorts, and equal or greater than with previously identified targets including *FOXO1*. Biochemical tests established that miR-96 binds directly to multiple target sites contained within the 3'UTR of *RARG* and using the bi-miR approach revealed ~400 direct targets enriched for predicted miR-96 target sequences, and identified targets were directly bound and downregulated upon miR-96 overexpression.

Experimental over-expression of miR-96 positively regulated proliferation and cell cycle in PCa cells reflecting previous reports(53,76), but did not affect proliferation in non-malignant prostate cells. It is thus interesting to speculate that miR-96 acquires additional targets and subsequent functions within the malignant transcriptome, which coincides with the observation of 3-fold additional targets in malignant LNCaP cells relative to non-malignant RWPE1, and impacts the control of cell cycle progression. Given that RARγ appears to function as an important AR co-regulator to promote differentiation, then its downregulation by miR-96 targeting suggests an oncogenic action that shifts the AR signaling capacity in localized PCa. Notably, miR-96 has previously been reported as androgen regulated in prostate cells(79). Filtering miR-96 target genes to those most altered in PCa revealed that nearly one third (7/22) were within an RARγ-centric network of co-regulators, suggesting its regulation as an important aspect of miR-96 function.

Differential expression analyses in TCGA-PRAD cohort between tumors showing reciprocal expression of miR-96 and RARγ/TACC1 clustered aggressive tumors and predicted worse disease free patient survival. Several of these genes are either under-explored in PCa (i.e. SOX15 and MCC) or have only been investigated in metastatic PCa(80,81) (PPARGC1A). Together these date strongly support the concept that the miR-96/RARγ is a significant and yet under-explored regulator of the AR and drives PCa progression.

METHODS

Data analyses and integration

All analyses, were undertaken using the R platform for statistical computing (version 3.1.0) (82) and a range of library packages were implemented in Bioconductor(83).

Cell culture and materials.

All cells were maintained in standard conditions in media recommended by ATCC. 2µg/mL puromycin was used for selection of pGIPz-shRARG and BAC-RARG-EGFP containing cell lines.

Cell proliferation and cell cycle analyses.

Bioluminescent detection of cellular ATP (proliferation) and cell-cycle distribution was determined utilizing FACSCalibur™ Flow Cytometer (Becton-Dickinson) and software.(16)

RT-qPCR.

Quantitative real-time reverse transcription–polymerase chain reaction (RT-qPCR) undertaken via Applied Biosystems 7300 Real-Time PCR System (Applied Biosystems), for both TaqMan® and SYBR® Green (SYBR® Green PCR Master Mix (Thermo Fisher Scientific)) applications(16). Fold changes were determined using the $2^{-\Delta\Delta Ct}$ method. Significance of experimental comparisons was performed using Student's t-test.

Western Immunoblotting

Western blot analysis of protein expression was undertaken as described previously (84). Membranes were probed with primary antibody against RARγ (sc550, Santa Cruz), GFP (ab290, Abcam or 2555S, Cell Signaling), or p27 (D37H1, Cell Signaling), either overnight at 4°C or for 3 hr at room temperature.

Expression determination in PCa mouse models

Snap frozen tissue and/or RNA from previously harvested normal or malignant prostate tissues of Hi-MYC, PTEN-/- and TRAMP (6, 8, 10, 15, 20-25 week) models, as well as from age-matched wild type (FVB:BL6, C57BL/6) mice, was obtained from the lab of Dr. Barbara Foster at RPCI. Relative expression of *Rarg* and microRNAs was determined in these tissues by RT-qPCR after normalization to *Gusb* or RNU6B, respectively.

miRNA mimic, antagomiR and siRNA transfection

Ectopic overexpression of miRNA was achieved by transient transfection of mirVana® miRNA mimics (30nM) (Ambion). Inhibition of miRNA was achieved by transient transfection of Anti-miR™ miRNA Inhibitor (30nM) (Ambion). For transient silencing of targets, siRNA was employed using Silencer® predesigned siRNAs (30nM) (Ambion). Transfection was accomplished by use of Lipofectamine® 2000 or Lipofectamine® 3000 by manufacturer's instructions. Concentrations of miRNA mimics and transfection reagents were optimized using BLOCK-iT™ Alexa Fluor® Red Fluorescent Control (Ambion) as well as by subsequent miRNA specific RT-qPCR and RT-qPCR of target mRNAs to assess efficiency of transfections.

RPCI PCa samples

RNA was obtained from a cohort of 36 men who underwent radical prostatectomy at RPCI and de-identified tissue made available through the Pathology Resource Network (PRN) and Data Bank and BioRepository (DBBR) shared resources at RPCI. Areas of histologically normal tissue and areas with high percentages of neoplastic tissue were isolated and RNA extracted. De-identified patient codes were matched with Gleason scores for each sample, were made available through the RPCI Clinical Data Network (CDN).

Molecular Cloning / Luciferase Assay

Luciferase assay was employed to assess direct targeting of miR-96 to the full length (FL) RARG 3'UTR or individual predicted target sites (t1, t2) within the RARG 3'UTR. RSV-pGL3-basic firefly luciferase expressing vector (Addgene) was employed for this purpose, utilizing FseI and XbaI restriction sites located between the *luc*+ gene and the SV40 pA tail. Primer sets were designed for PCR amplification of either the ~1100bp full-length (FL) *RARG* 3'UTR or two smaller regions (~300bp) within the *RARG* 3'UTR containing individual predicted miR-96 target sites (t1, t2). PCR amplicons were digested and ligated to RSV-pGL3-basic vector via T4 DNA Ligase in 1X T4 DNA Ligase Buffer (New England BioLabs, Inc.), using an insert to vector ratio of 2.6. Individual transformed *E.coli* colonies were expanded prior to plasmid isolation via E.Z.N.A® Plasmid Mini Kit (Omega), and inserts verified by sanger sequencing. RWPE1 cells were seeded in 96-well plates and then co-transfected with combinations of miR-96 or miR-control mimics (30nM), indicated RSV-pGL3 constructs (250ng), and pRL-CMV Renilla luciferase expressing vectors (25ng) via Lipofectamine® 2000 for 48 hr. Media was subsequently removed, cells washed with PBS, and both firefly and Renilla luciferase activity measured by Dual-Glo Luciferase Assay System (Promega). For each construct (FL, t1, t2,

empty), detected firefly luminescence was first normalized to Renilla luminescence, and then normalized luminescence was compared between miR-96 and miR-control transfected cells. Experiments were performed in technical triplicates, and experiment replicated a total of 5 times.

Stable knockdown of RARγ

Knockdown of RARγ in RWPE1, LNCaP and HPr1AR cells was achieved by stable selection after transduction with lentiviral shRNA constructs targeting *RARG*. Two targeting constructs (V2LHS_239272, V2LHS_239268) and one non-silencing control construct were selected from the V2LHS pGIPZ based lentiviral shRNA library (Thermo Fisher Scientific) for testing. Viral packaging and cellular infection was performed through the RPCI shRNA Resource. All pGIPZ containing cells were subsequently maintained in media supplemented with puromycin (2μg/mL), including during all experiments.

RWPE1-BAC-RARG-EGFP

BAC-RARG-EGFP construct (CTD-2644H7) was a generous gift of Dr. Kevin White (University of Chicago). RWPE1 cells were transfected with BAC-RARG-EGFP construct using Lipofectamine® 3000 and selected with G418 and consistently maintained under antibiotic selection for all subsequent passaging of cells and also during experiments.

Chromatin Immunoprecipitation

ChIP was performed in BAC-RARG-EGFP containing RWPE1 cells in the presence of CD437 (10nM, 2hr) or DMSO as previously described(16). The RARγ cistrome was analyzed with `Rsubread/csaw`(85,86), along with TF motif analyses (`MotifDb`). Binding site overlaps between RARγ and the other cistromes tested (`ChIPpeakAnno` and `bedtools`).

Biotin-miRNA pulldown

Approximately 20 million cells were transfected with either hsa-miR-96-5p or cel-miR-67 miRIDIAN miRNA mimics (30nM, 24hr) modified with a 3'biotin attached to the guide strand (Thermo Fisher Scientific) using Lipofectamine® 3000 Transfection Reagent (Invitrogen). Harvested cell pellets were resuspended in cell lysis buffer (10mM KCl, 1.5mM MgCl2, 10mM Tris-Cl pH 7.5, 5mM DTT, 0.5% Sigma-IGEPAL CA-630) containing SUPERase·In (Ambion) and 1x cOmplete Mini protease inhibitor (Roche) and cleared by centrifugation. 5% of cell lysate was collected to serve as lysate RNA input. Dynabeads® MyOne™ Streptavidin C1 (Thermo Fisher Scientific) were washed 3 times with bead wash buffer (5mM Tris-Cl pH 7.5, 0.5mM

EDTA, 1M NaCl), and then blocked (1μg/μL bovine serum albumin, 1μg/μL Yeast tRNA, 50U/mL RNaseOUT) for 2 hr. Resuspended beads were added 1:1 to cell lysate, and mixed for 30 minutes. Bead-lysate mixtures were collected with a magnetic rack, and bead-bi-miR complexes washed a total 3 times with wash buffer. Bead-bi-miR complexes and input control samples were resuspended in water and purified using the Qiagen RNeasy® Mini kit (Qiagen) according to manufacturer's RNA clean-up protocol. To concentrate samples for downstream analyses, eluted RNA was brought up to a total volume of 500μL in H_2O and filtered through Amicon® Ultra-0.5mL Centrifugal Filters (EMD Millipore) according to manufacturer's instructions. Subsequent amplification and labeling of 50ng of pulldown and input RNA was performed at the Roswell Park Cancer Institute Genomics Core Facility, using the Illumina® TotalPrep RNA Amplification kit, including a 14 hour incubation for the IVT step. Hybridization of cRNA samples onto the Illumina® Human HT-12v4 bead arrays, and successive scanning and raw intensity measurement extraction were also performed at the RPCI Genomics Core Facility.

miRNA prediction determination & TCGA miRNA analysis

To reveal putative NR-targeting miRNA, miRWalk, a comprehensive database on predicted and validate miRNA targets, was employed. If at least 5 out of 9 algorithms positively predicted an interaction, it was considered in subsequent analyses. MiRNA expression was queried in PCa tissue samples and matched normal tissue from TCGA cohort data as previously described(27). To examine if NR-targeting miRNA expression alterations significantly deviated from what would be expected by chance, bootstrapping permutation approaches were utilized As previously described(27).

Microarray / RNA-seq analyses

Global changes in mRNA, biological triplicate samples per experimental condition were analyzed using Illumina microarray (Illumina HT12v4) or by RNA-seq (`limma`(87) or `DESeq2`(88)). For RNA-seq data, raw sequence reads were aligned to the human genome (hg19) using `tophat2`, and aligned reads translated to expression counts via `featurecounts`, followed by a standard `DESeq2` pipeline.

Functional annotation of shRARG defined gene sets

Functional annotations were performed using GSEA v3.0 and gene sets from the Molecular signatures database (MSigDB). Specifically, gene sets were compiled to assess enrichment of all BROAD Hallmark pathways, curated pathways (KEGG, BioCarta, Canonical, Reactome, Chemical/Genetic perturbations), and transcription factor motif gene sets. Additionally, several

candidate gene sets were included from previous studies, including microarray analyses of HPr1AR cells treated with DHT(89), compiled gene sets previously utilized to encompass androgen response in PCa patients(34), as well as gene sets differentiating basal from luminal prostate epithelial cells(90). In total, 4204 gene sets were queried. To identify meta groups within enriched (NES > 1.8, FDR q-val < 0.05) gene sets, keywords from gene set identifiers were compiled, and frequency tables determined for all keywords across all gene sets and within enriched gene sets. Hypergeometric testing was used to determine if the frequency of key words within enriched gene sets was greater than expected.

Validation of miR-96 target sites & Functional annotation

Unbiased assessment of miRNA seed sequence binding motifs in experimentally determined miR-96 target transcript 3'UTR regions was performed using the MSigDB microRNA targets collection.Functional annotation of GO terms enriched in miR-96 target genes was accomplished via DAVID Bioinformatics Resources 6.7 (via BiNGO) and additionally by the topGO package implemented in R. Significantly enriched terms (FDR < 0.05) by both methods were simultaneously visualized using Cytoscape 3.2.0.

AUTHORS CONTRIBUTIONS

Acknowledgements

LESC acknowledges support, in part, of Roswell Park Cancer Institute-University of Pittsburg Cancer Institute Ovarian Cancer Specialized Program of Research Excellence National Institutes of Health [P50CA159981-01A1].

MDL acknowledges support of Molecular Pharmacology and Experimental Therapeutics NRSA T32 program [T32CA009072] held at Roswell Park Cancer Institute.

MJC and *DJS* acknowledges support in part from the Prostate program of the Department of Defense Congressionally Directed Medical Research Programs [W81XWH-14-1-0608, W81XWH-11-2-0033] and the National Cancer Institute (NCI) grant P30CA016056 involving the use of Roswell Park Cancer Institute's Genomic Shared Resource.

MJC, GL, AR, HW and *PvdB* acknowledges support from the European Union-United States Atlantis Program [P116J090011].

MJC and *LESC* acknowledge support from the National Cancer Institute (NCI) grant P30CA016056 involving the use of OSUCCC The James, CCSG P30CA016058

RARγ State	Motif	Enrich.	E-Value
Apo	FOSB JUNB JUN	MEME	1.2e-80
	OTX2 PITX2 PITX1	MEME	9.2e-12
	RARB RARA RARG	MEME	2.4e-9
	ELF3 TFDP1 STAT1	MEME	3.2e-7
Holo	CPEB1 ONEC2 HXC10	MEME	1.5e-14
	FOSB JUNB JUN	MEME	3.3e-12
	HIC2 RREB1 PAX5	MEME	6.1e-7

Table 1: Summary of top motif enrichments in significant RARγ binding sites identified from ChIP-seq.

	Number of events	
	Apo-RARγ	*Holo*-RARγ
(A) RARγ DEG	1717	731
(B) RARγ cistrome peaks	1256	360
(C) RARγ peaks annotated to genes	512	155
(D) Annotated RARγ cistrome genes expressed in RWPE-1	159	40
(E) Overlap A & D	38	18
(F) RARγ DEG genes detected in TCGA-PRAD	663	201
(G) Top 10 significant GSEA for (F)	PUJANA_BRCA1_PCC_NETWORK PILON_KLF1_TARGETS_DN PUJANA_ATM_PCC_NETWORK PUJANA_CHEK2_PCC_NETWORK DODD_NASOPHARYNGEAL_CARCINOMA_DN 1375 JOHNSTONE_PARVB_TARGETS_3_DN KRIGE_RESPONSE_TO_TOSEDOSTAT_24HR_DN NUYTTEN_EZH2_TARGETS_DN PUJANA_BRCA2_PCC_NETWORK MARSON_BOUND_BY_E2F4_UNSTIMULATED	GRAESSMANN_APOPTOSIS_BY_DOXORUBICIN_UP DELYS_THYROID_CANCER_UP GRAESSMANN_RESPONSE_TO_MC_AND_DOXORUBICIN_UP KOINUMA_TARGETS_OF_SMAD2_OR_SMAD3 BILD_HRAS_ONCOGENIC_SIGNATURE 261 DELACROIX_RARG_BOUND_MEF BRUINS_UVC_RESPONSE_VIA_TP53_GROUP_B SHETH_LIVER_CANCER_VS_TXNIP_LOSS_PAM1 GCGCCTT_MIR525_MIR524 ONDER_CDH1_TARGETS_2_DN

Table 2: Summary of overlaps of the apo and holo RARγ cistrome and transcriptomes. (A). Differentially expressed genes (log fold change 1.2, p.adj =0.1) in RWPE1 cells following shRNA to RARγ (*Apo*-RARγ) or treatment with CD437 (*Holo*-RARγ) and detected by microarray analyses (B). Significant RARγ bound peaks (p.adj < 0.1) in RWPE-1. (C). RARγ bound genes

were annotated to +/- 7.5 kb TSS of known genes. (D) Unique RARγ bound genes that are detected by in RWPE-1 microarray expression set. (E) Overlap of RARγ regulated genes and RARγ bound genes. These sets were used for bootstrap analyses to test significance of relationship between RARγ binding and gene expression. (F) Number of RARγ-dependent DEGs expressed in more than 80% tumors compared to normal samples in the TCGA-PRAD. (G) Top 10 significant GSEA terms for (F).

Figure Legends

Figure 1: RARγ has retinoid dependent and independent regulatory function in prostate cells. (**A**) Relative proliferation of shRARG clones compared to vector controls in RWPE1 (left) and LNCaP (right) cells over time. Significant differences are indicated between control and RARγ knockdown cells ($p < 0.05$). (**B**) Cells were treated in triplicate with CD437 (RWPE1 - 10 nM; LNCaP- 250 nM, 24hr) or vehicle control and gene expression profiled via Illumina microarray (Illumina HT12v4). Volcano plots depicting expression changes upon RARγ knockdown (*apo* RARγ) or in response to RARγ specific ligand (CD437) (*holo* RARγ) in RWPE1 cells. Dotted lines indicate DEG thresholds (p.adj < 0.05, fold change of +/- 1.2), and red dots represent RARγ dependent DEGs. *Holo* RARγ were those genes that were significant in shCTL cells (shCTRL-CD437/shCTRL-DMSO) and not in shRARG cells cells. (**C**) Venn diagram depicting number of determined DEGs associated with *apo* RARγ and *holo* RARγ conditions. (**D**) Summary of significantly enriched pathways from GSEA (NES > 1.8, FDR q.val < 0.05) associated with *apo* RARγ and *holo* RARγ conditions in RWPE1 and LNCaP cells. Example enriched meta-groups amongst significant GSEA sets are indicated. (**E,F**) Examples of top significant GSEA pathway enrichments observed in RWPE1 cells and (**G**) in LNCaP cells. (**H**) Heatmap depicting the relative expression of a panel of androgen response genes defined previously by the TCGA consortium to reflect AR signaling(78).

Figure 2: The RARγ cistrome associates with androgen receptor and regulates genes associated with aggressive prostate cancer. Stable transfection of a bacterial artificial chromosome containing a fusion *RARG-EGFP* gene transcribed from the endogenous *RARG* promoter was undertaken to generate RWPE1-RARG-EGFP clones, followed by ChIP-Seq undertaken with an EGFP antibody. RWPE1-RARγ-EGFP cells were treated in triplicate with either CD437 (10 nM, 2 hr) or vehicle prior to ChIP-seq. (**A**) Venn diagram depicting the significant RARγ cistrome (binding peaks; p.adj<0.01) in *holo* and *apo* RARγ. (**B**) Overlap of RARγ cistrome with publically available epigenetic datasets (H3K4me1 and H3K27ac (GSE63094) and DNAse sensitivity (GSM1541008). (**C**) Significance of *apo* RARγ peaks with publically available data; prostate enhancers (FANTOM (ref); LNCaP AR (ref), VCaP AR (ref), ERα (ref) and LNCaP NF-κB cistromes(91,92) (**D**) Illustration of binding site at the TSS of the KRT15 gene showing coincident binding with H3K4me1 and H3K27ac in RWPE-1 cells, the ChromHMM track (grass green = ; bright green = ; red = ; blue = ; pale yellow = ; yellow = ; blue = . (**E**). the impact of RARγ knockdown on KRT15 from the microarray experiment in RWPE-1 cells (**Figure 1**). (**F**). Bootstrapping approach to test the statistical strength of relationships

between genes annotated to be bound by RARγ (+/- 7.5 kb from the TSS) and modulated by shRARG (left) or in the presence of ligand (right). The red line is the mean observed fold change for the indicated gene set and the distribution is simulated data from the same background. (**G**). Heatmap of expression of annotated *apo* RARγ cistrome genes in the TCGA-PRAD cohort. Genes were filtered to identify those that were altered by more than 2 Zscores in 35% of tumors relative to normal samples. Cluster association grouped tumors that significantly distinguished higher Gleason Grade (>7). For each gene Kaplan-Meier curves were generated as time to biochemical progression and those genes which identify significantly shorter disease free survival are indicated. (**G**). Illustrative Kaplan-Meier curve for *CYP11A1* expression depicting the significantly reduced time to 5 year biochemical recurrence post radical prostatectomy.

Figure 3: RARγ governs androgen induced responses in non-malignant HPr1AR prostate epithelial cells. (**A**) Proliferation of HPr1AR-shCTL and HPr1AR-shRARG cells with or without the presence of 10 nM DHT for up to 96 hours. (**B**) HPr1AR-shCTL and HPr1AR-shRARG cells were treated in triplicate with DHT for 24h or vehicle control and gene expression profiled via RNA-seq. Volcano plot depicting DHT induced (10 nM, 24 hr) gene expression changes in HPr1AR-shCTL cells. Genes marked in red represent those that displayed differential regulation in RARγ knockdown cells. (**C**) Venn diagram representing the number of DEGs determined after DHT treatment in control and RARγ knockdown HPr1AR cells. (**D**) Heatmap depicting all enriched pathways related to DHT treatment (NES > 1.8, FDR q-val < 0.05). Select meta groups from keyword enrichment analysis are depicted as row annotations. The definitions of the groups are as follows; shCTL+DHT = shCTL+DHT/shCTL+EtOH, shRARG+DHT = shRARG+DHT/shRARG+EtOH, Apo-RARG (+DHT) = shRARG+DHT/shCTL+DHT.(**E**) Example of top significantly upregulated and (**F**) downregulated GSEA pathway enrichments upon DHT treatment. Enrichments are shown for each comparison, as well as an expression profile from a select gene from the respective gene set.

Figure 4: MicroRNA-96 directly targets and regulates *RARG* in prostate cells. (**A**) Cross-correlation matrices depicting the relationships between RARG expression and miR-96 cluster members in PCa samples from either MSKCC or TCGA-PRAD cohorts. (**B**) Relative expression of miR-96 (bottom) and *RARG* (top) across 10 prostate cell lines representing different stages of PCa progression. The cell models examined comprised immortalized RWPE1 and HPr1AR non-malignant prostate epithelial cells, LNCaP, LAPC4 and EAA006 androgen sensitive PCa cells, MDAPCa2b, 22Rv1 and LNCaP-C42 CRPC cells, as well as PC3 and DU145 cells derived from

distant metastases. (**C**) Correlation analyses of *RARG* with miR-96 over the course of palpable tumor (PT) development in TRAMP. (**D**) *RARG* expression (left panel) and RARγ protein expression (right panels) in RWPE1 cells after 48 hr transfections with miR-96 mimics or siRNA targeting *RARG*. (**E**) Luciferase assay assessing direct targeting of miR-96 to the full length (FL) RARG 3'UTR or individual predicted target sites (t1, t2) within the RARG 3'UTR. Either miR-96 or miR-CTL mimics (30 nM) were transfected into RWPE1 cells for 48 hours along with indicated RSV-pGL3 constructs and pRL-CMV Renilla luciferase expressing vectors, and luciferase activity measured by Dual-Glo Luciferase Assay System. (**F**) RWPE1 cells were pretreated with miR-CTL, miR-96 mimic (30 nM), or combination of miR-96 mimic and antagomiR-96 for 48 hours prior to 10 nM CD437 exposure for 24 hours, and candidate transcripts measured by RT-qPCR. Induction relative to untreated control for each condition is shown, and significance relative to shCTL is noted. (**G**) Cell proliferation was measured in RWPE-1 (left) and LNCaP (right) cells for up to 120 hours post-transfection with either miR-96 or non-targeting control (NC) mimics.

Figure 5: The miR-96 targetome centers on a RARγ-network associated with aggressive prostate cancer (**A**) LNCaP cells were transfected with bi-miR-96 or bi-cel-miR-67 (non-targeting control, bi-miR-NC) (30 nM) 24 hr prior to cell lysis. From triplicates, input (5% of cell lysate) and streptavidin pulldown RNA were isolated and analyzed by Illumina microarray (Illumina HT12v4). Volcano plot depicting the enrichment of all genes in bi-miR-96 pulldown over input in LNCaP cells. Genes marked in red (n = 389) were considered experimentally determined miR-96 direct targets, as they were significantly enriched (FC > 1.2, p.adj < 0.05) in bi-miR-96 pulldown but not in bi-miR-NC pulldown. (**B**) Venn diagram representing the overlap of miR-96 targetomes in LNCaP and RWPE1 cells. (**C**) Example of top significantly enriched GSEA pathway from unbiased enrichment analysis of bi-miR-96 samples in LNCaP cells (pulldown/input) (left), and summary of top miRNA seed sequence matches in 3'UTR regions of experimentally determined miR-96 targets using the GSEA-MSigDB microRNA targets tool (right). (**D**) Either bi-miR-96 or non-biotinylated miR-96 mimics, and respective control mimics, were transfected (30nM) in LNCaP cells for 48 hr and target gene expression examined. *CDH1* was assessed as a negative control, and specific targets were chosen either as they were either previously validated (*FOXO1*, *RARG*) and were significantly enriched in bi-miR assay. Significance is noted (p < 0.05), for comparisons of target transcripts in biotinylated (#) and non-biotinylated miR-96 (*) relative to respective controls. (**E**) Cumulative distribution plot comparing the correlations (Pearson's r) between miR-96 and all detectable genes from bi-miR-pulldown assay (n = 10,827, black) in TCGA-PRAD cohort samples to the correlations of validated targets

(n = 389, red) across the same samples. Significant difference between distributions is determined by Kolmogorov-Smirnov test. (**F**). Heatmap depicting expression of annotated LNCaP miR-96 targetome genes in the TCGA-PRAD cohort. Genes were filtered to identify those genes that were altered by more than 2 Zscores in 35% of tumors relative to normal samples. Cluster association grouped tumors into groups that significantly distinguished invasive tumors (Pathological N0 or N1). For each gene Kaplan-meier curves were generated as time to biochemical progression and those genes which identify significantly shorter disease free survival are indicated. Also indicated is the functional relationship of the gene to RARγ as membership of the RARγ network. (**G**). Illustrative Kaplan-meier curve for *TACC1* expression depicting the significantly reduced time to 5 year biochemical recurrence post radical prostatectomy.

Figure 6: A miR-96/RARγ network associates with aggressive prostate cancer. (**A**) TCGA-PRAD cohort tumor samples were separated based on expression of RARγ, TACC1 and miR-96 (based on lower/upper tertile expression) to generate RARγ/TACC1$_{low}$, miR-96$_{high}$ (n = 60) and RARγ/TACC1$_{high}$, miR-96$_{low}$ (n = 66) tumors and differential expression undertaken (`limma`). (**B**) Filtering the differentially expressed 1728 gene sets as in **Figure 2G** revealed which were most altered in the TCGA-PRAD cohort. These are represented as a heatmap in which tumor clusters significantly associated, after adjusting for age, with high Gleason grade ($p<0.012$). These clusters also significantly identified patients who experienced treatment failure and worse disease free survival following radical prostatectomy (log-rank test p-val = 0.026). Individual genes were annotated by their relationship to survival outcome, RARγ binding, RARγ-dependent AR regulation, and enrichment in the Liu prostate cancer gene set. (**C**) SOX15 is bound by RARγ and also a RARγ-dependent AR regulated target. (**D**) PPARGC1A independently associated with worse disease free survival.

Supplementary Figure 1: (**A**) Validation of *RARG* mRNA and (**B**) RARγ protein knockdown in RWPE1-shCTL and RWPE1-shRARG cells. (**C, D**) Similar validation results are shown for LNCaP-shCTL and LNCaP-shRARG cells. (**E**, **F**) Representative bright-field and fluorescent images of parental and pGIPz-shRNA containing RWPE1 and LNCaP cells, respectively.

Supplementary Figure 2: Dose response curves were generated in RWPE1-shCTL and RWPE1-shRARG cell lines in responses to ATRA (**A**) and CD437 (**B**) for 96 hours. Significant differences in response relative to RWPE1-shCTL cells are indicated ($p < 0.05$). (**C,D**) Similar results shown for LNCaP-shCTL and LNCaP-shRARG cells treated for 144 hours. (**E**) Representative propidium iodide profiles of RWPE1-shCTL and RWPE1-shRARG cells treated with vehicle, 1 μM ATRA or 10nM CD437 for 96 hours. Cell cycle phase populations were determined by ModFit 3.1 software. Quantification of cell cycle profiles from triplicate experiments are shown below. Asterisks denote significant shifts in populations in shRARG cells relative to control cells in each treatment group (Student's t-test, $p < 0.05$). (**F**): Similar results shown for LNCaP-shCTL and LNCaP-shRARG cells treated with vehicle, 1 μM ATRA or 250nM CD437 for 120 hours.

Supplementary Figure 3: (**A**) Principal component analysis depicting relationships amongst samples profiled by microarray in RWPE1 cells and (**B**) LNCaP cells. (**C**) Volcano plots depicting expression changes upon RARγ knockdown (*apo* RARγ) or in response to RARγ specific ligand (CD437) in LNCaP cells. dotted lines indicate DEG thresholds (p.adj < 0.05, fold change of +/- 1.2), and red dots represent RARγ dependent DEGs. (**D**) Venn diagram depicting number of determined DEGs associated with *apo* RARγ and *holo* RARγ conditions. (**E**) (**F**) Heatmap depicting a summary of all significantly enriched pathways from GSEA (NES > 1.8, FDR q.val < 0.05) associated with *apo* RARγ and *holo* RARγ conditions in RWPE-1 and LNCaP cells. Example enriched meta-groups amongst significant GSEA sets are shown as row annotations. (**G**) Expression of typical androgen regulated genes *KLK3* and *TMRPSS2* in RARγ knockdown LNCaP cells treated with 10nM DHT for 24 hours. Significant expression changes relative to LNCaP-shCTL DMSO treated cells is indicated ($p < 0.05$).

Supplementary Figure 4: Validation of stable BAC-RARG-EGFP expressing cells. (**A**) RARG transcript is detected at significantly elevated levels in RWPE1-BAC-RARG-EGFP cells relative to basal RWPE1 cells. (**B**) Detection of RARG-EGFP corresponding fusion protein in RWPE1-BAC-RARG-EGFP cells by use of GFP targeting antibody. RWPE1 cells containing pGIPz-shRNA vectors are used as control for detection of wild type GFP. (**C**) Candidate ChIP-qPCR in RWPE1-BAC-RARG-EGFP cells either treated with DMSO or 10nM CD437 for 2 hours

at TSS regions of genes regulated by RARγ in RWPE-1 cells (CYP26A1, KRT8/18, CDKN2B, FOXA1, SMAD3) or negative control TSS regions at genes not regulated by RARγ.

Supplementary Figure 5: MiR-96 expression in MSKCC and TCGA-PRAD cohorts. A. Cumulative distribution plot comparing the correlations (Pearson's r) between RARγ and all detectable genes from ChIP-Seq assay in cohort samples to the correlations of validated targets (red) across the same samples in TCGA-PRAD (left) and MSKCC (right). Significant difference between distributions is determined by Kolmogorov-Smirnov test. **B**. Filtering these gene sets as revealed which were most altered in the MSCKCC cohort. Several of these genes were independently associated with worse disease free survival

Supplementary Figure 6: (**A**) Validation of *RARG* mRNA and (**B**) RARγ protein knockdown in HPr1AR-shCTL and HPr1AR-shRARG cells. (**C**) Protein levels of RARγ are unaffected by DHT treatment (10 nM, 24 and 96 hours). (**D**) Expression of *RARG* transcript and other candidate DHT regulated genes (*DPP4*, *STEAP4*, *S100P*) in HPr1AR cells.

Supplementary Figure 7: (**A**) Principal component analysis depicting relationships amongst samples profiled by RNA-seq in HPr1AR cells. (**B**) Volcano plot representing the identification of RARg dependent DHT induced (96hr) gene expression changes in HPr1AR cells. (**C**) Corresponding venn diagram. (**D**) Genomic locus including MYC TSS, depicting an upstream enhancer region with RARγ binding.

Supplementary Figure 8: Matching normal tissue relative DNA methylation changes in tumors from the TCGA-PRAD cohort. Each data point represents the average relative change in methylation for a given CpG site. The genomic loci for RARG (top), RARA (middle) and RARB (bottom) are shown. CpG islands are delineated in purple. The genomic distance (bp) and direction are indicated for each loci.

Supplementary Figure 9: (**A**): Putative NR targeting miRNA, identified via miRWalk, were compiled and normal tissue relative expression alterations determined in both TCGA-PRAD and MSKCC cohorts. (**B**): Bootstrapping analysis comparing expression alterations associated with putative NR targeting miRNA relative to all expressed miRNA in the MSKCC cohort.

Supplementary Figure 10: (**A**) Venn diagram comparing the number of predicted targets of members of the miR-96-182-183 cluster as determined by miRWalk. (**B**) Diagram depicting the *RARG* transcript and putative miR-96 target sites within the 3'UTR.

Supplementary Figure 11: (**A**) To address if and/or which murine models would serve as potential models to profile expression changes during development of PCa which was relevant

to expression changes observed in human PCa cohorts, diseased prostate tissue was obtained from Hi-MYC, PTEN-/- and TRAMP mice and Rarg expression determined by RT-qPCR. Significant expression changes are indicated relative to wild type (WT) FVB:BL6 mice ($p < 0.05$). (**B**) Correlation analyses of *RARG* with miR-182 and miR-183 over the course of palpable tumor (PT) development in TRAMP. Time points are denoted by color. Pearson's correlation coefficients are indicated for each comparison, as well as the significance of correlations.

Supplementary Figure 12: (**A**) Summary of expression changes observed within an independent cohort of 36 matched tumor/normal prostate samples (RPCI) in relation to matching tumor/normal pairs from the TCGA-PRAD and MSKCC cohorts. Significance of expression changes in each case was determined via one sample t test. (**B**) Profile of expression changes in each tumor/matching normal pair relative to the Gleason sum for that patient in the RPCI cohort. (**C**) miR-96 expression significantly increases with increasing Gleason sum and clinical stage within the TCGA-PRAD cohort. (**D**) Kaplan-meier curves depicting the significantly reduced time to 5 year biochemical recurrence post radical prostatectomy in men with elevated miR-96 expression.

Supplementary Figure 13: (**A**) Validation of elevated miR-96 levels in RWPE1 cells and in (**B**) LNCaP cells after 48 hour transfection with miR-96 mimics. (**C**) *RARG* mRNA expression (left panel) and RARγ protein expression (right panels) in LNCaP cells after 48 hour transfections with miR-96 mimics or siRNA targeting RARG.

Supplementary Figure 14: Cell cycle distributions were assess in RWPE-1 (left) and LNCaP (right) cells 48 hours post-transfection with miR-96 or non-targeting control mimics. Significant differences in miR-96 mimic transfected cells relative to control cells is indicated ($p < 0.05$).

Supplementary Figure 15: (**A**): biotin labelled miR-96 is detectable at elevated levels relative to biotin labelled miRNA control by miRNA specific RT-qPCR after 24 hours of transfection in RWPE1 cells. (**B**): bi-miR-96 transfection results in predictable loss of RARγ expression in RWPE1 cells. (**C**) Enrichment of known (*RARG*, *FOXO1*) and highly predicted (*TBL1X*) candidate targets after bi-miR-96 pulldown followed by RT-qPCR in RWPE1 cells. (**D**) Unsupervised hierarchical clustering of samples profiled for miR-96 target identification study. (**E**) Volcano plot depicting the enrichment of all genes in bi-miR-96 pulldown over input in RWPE1 cells. Horizontal lines indicate an adjusted p-value = 0.05, and vertical lines indicate fold change of +/- 1.2, shown for reference. Genes marked in red (n = 111) were considered experimentally determined miR-96 direct targets, as they were significantly enriched in bi-miR-96 pulldown but not in bi-miR-NC pulldown. (**F**) A panel of genes was selected to assess the

technical validity of target enrichment determined by microarray in LNCaP cells. Enrichment determined by microarray (left) is directly compared to enrichment determined by RT-qPCR (right). Statistically significant enrichment is indicated ($p < 0.05$). (**G**) Western blot showing p27 (*CDKN1B*) knockdown in LNCaP cells transfected with miR-96 for 48 hr. Representative blot shown (upper) with quantitation of triplicate blots (lower). (**H**) Either bi-miR-96 or non-biotinylated miR-96 mimics, and respective control mimics, were transfected in RWPE1 cells for 48 hr and target gene expression examined. *CDH1* was assessed as a negative control, and specific targets were chosen either as they were either previously validated (*FOXO1*, *RARG*) were significantly enriched in bi-miR-chip assay. Significance is noted ($p < 0.05$), for comparisons of target transcripts in biotinylated-miR-96 (#) and non-biotinylated miR-96 (*) relative to respective controls.

Supplementary Figure 16: (**A**) Significant GO terms (adjusted $p < 0.05$) identified by cross-referencing miR-96 targets with curated gene sets associated with biological processes using DAVID Bioinformatics Resource 6.7 (blue) and topGO (red). Gene sets with similar annotations were grouped together and visualized using Cytoscape 3.2.0. Annotations not fitting into hierarchical groupings are placed under 'Biological Processes'. (**B**) Diagram depicting strategy for revealing clinically meaningful miR-96-target relationships from GO term gene sets. As an example, a total of 38 miR-96 targets were found within enriched cell cycle related GO-terms. Correlations between these 38 genes and miR-96 were calculated across TCGA-PRAD cohort samples, for instance as seen for TACC1. The top 5 most significant, negative correlations were profiled for miR-96 regulation by RT-qPCR. This approach was applied to genes associated with cell cycle as described (**C**), and also for genes with functional annotations associated with transcription factors (**D**)

Supplementary Figure 17: Euler diagrams of publicaly available (GSE31280) transcriptomes in ES (top) or F9 (bottom) cells with RARγ -/- and treated with ATRA. Data were processed with limma and the circles represent the size and overlaps of the indicated transcriptomes.

References

1. Wang J, Zou JX, Xue X, Cai D, Zhang Y, Duan Z*, et al.* Corrigendum: ROR-gamma drives androgen receptor expression and represents a therapeutic target in castration-resistant prostate cancer. Nat Med **2016**;22(6):692 doi 10.1038/nm0616-692b.
2. Yu Y, Lee JS, Xie N, Li E, Hurtado-Coll A, Fazli L*, et al.* Prostate stromal cells express the progesterone receptor to control cancer cell mobility. PLoS One **2014**;9(3):e92714 doi 10.1371/journal.pone.0092714.
3. Lin SJ, Lee SO, Lee YF, Miyamoto H, Yang DR, Li G*, et al.* TR4 nuclear receptor functions as a tumor suppressor for prostate tumorigenesis via modulation of DNA damage/repair system. Carcinogenesis **2014**;35(6):1399-406 doi 10.1093/carcin/bgu052.
4. Long MD, Thorne JL, Russell J, Battaglia S, Singh PK, Sucheston-Campbell LE*, et al.* Cooperative behavior of the nuclear receptor superfamily and its deregulation in prostate cancer. Carcinogenesis **2014**;35(2):262-71 doi 10.1093/carcin/bgt334.
5. Mathieu R, Evrard B, Fromont G, Rioux-Leclercq N, Godet J, Cathelineau X*, et al.* Expression screening of cancer/testis genes in prostate cancer identifies NR6A1 as a novel marker of disease progression and aggressiveness. Prostate **2013**;73(10):1103-14 doi 10.1002/pros.22659.
6. Campbell MJ, Park S, Uskokovic MR, Dawson MI, Koeffler HP. Expression of retinoic acid receptor-beta sensitizes prostate cancer cells to growth inhibition mediated by combinations of retinoids and a 19-nor hexafluoride vitamin D3 analog. Endocrinology **1998**;139(4):1972-80 doi 10.1210/endo.139.4.5943.
7. Wilson S, Qi J, Filipp FV. Refinement of the androgen response element based on ChIP-Seq in androgen-insensitive and androgen-responsive prostate cancer cell lines. Sci Rep **2016**;6:32611 doi 10.1038/srep32611.
8. Chatagnon A, Veber P, Morin V, Bedo J, Triqueneaux G, Semon M*, et al.* RAR/RXR binding dynamics distinguish pluripotency from differentiation associated cis-regulatory elements. Nucleic Acids Res **2015**;43(10):4833-54 doi 10.1093/nar/gkv370.
9. Need EF, Selth LA, Harris TJ, Birrell SN, Tilley WD, Buchanan G. Research resource: interplay between the genomic and transcriptional networks of androgen receptor and estrogen receptor alpha in luminal breast cancer cells. Mol Endocrinol **2012**;26(11):1941-52 doi 10.1210/me.2011-1314.
10. Boergesen M, Pedersen TA, Gross B, van Heeringen SJ, Hagenbeek D, Bindesboll C*, et al.* Genome-wide profiling of liver X receptor, retinoid X receptor, and peroxisome proliferator-activated receptor alpha in mouse liver reveals extensive sharing of binding sites. Mol Cell Biol **2012**;32(4):852-67 doi 10.1128/MCB.06175-11.
11. Lu L, Wang J, Lu H, Zhang G, Liu Y, Wang J*, et al.* MicroRNA-130a and -130b enhance activation of hepatic stellate cells by suppressing PPARgamma expression: A rat fibrosis model study. Biochem Biophys Res Commun **2015**;465(3):387-93 doi 10.1016/j.bbrc.2015.08.012.
12. Sun J, Wang Y, Li Y, Zhao G. Downregulation of PPARgamma by miR-548d-5p suppresses the adipogenic differentiation of human bone marrow mesenchymal stem cells and enhances their osteogenic potential. J Transl Med **2014**;12:168 doi 10.1186/1479-5876-12-168.
13. Tombolan L, Zampini M, Casara S, Boldrin E, Zin A, Bisogno G*, et al.* MicroRNA-27a Contributes to Rhabdomyosarcoma Cell Proliferation by Suppressing RARA and RXRA. PLoS One **2015**;10(4):e0125171 doi 10.1371/journal.pone.0125171.
14. Duan JH, Fang L. MicroRNA-92 promotes gastric cancer cell proliferation and invasion through targeting FXR. Tumour Biol **2014**;35(11):11013-9 doi 10.1007/s13277-014-2342-x.

15. Zhong D, Zhang Y, Zeng YJ, Gao M, Wu GZ, Hu CJ*, et al.* MicroRNA-613 represses lipogenesis in HepG2 cells by downregulating LXRalpha. Lipids Health Dis **2013**;12:32 doi 10.1186/1476-511X-12-32.
16. Thorne JL, Maguire O, Doig CL, Battaglia S, Fehr L, Sucheston LE*, et al.* Epigenetic control of a VDR-governed feed-forward loop that regulates p21(waf1/cip1) expression and function in non-malignant prostate cells. Nucleic Acids Res **2011**;39(6):2045-56 doi 10.1093/nar/gkq875.
17. Kerr JF, Wyllie AH, Currie AR. Apoptosis: a basic biological phenomenon with wide-ranging implications in tissue kinetics. Br J Cancer **1972**;26(4):239-57.
18. Matusik RJ, Jin RJ, Sun Q, Wang Y, Yu X, Gupta A*, et al.* Prostate epithelial cell fate. Differentiation **2008**;76(6):682-98 doi 10.1111/j.1432-0436.2008.00276.x.
19. Malinen M, Niskanen EA, Kaikkonen MU, Palvimo JJ. Crosstalk between androgen and pro-inflammatory signaling remodels androgen receptor and NF-kappaB cistrome to reprogram the prostate cancer cell transcriptome. Nucleic Acids Res **2017**;45(2):619-30 doi 10.1093/nar/gkw855.
20. Starick SR, Ibn-Salem J, Jurk M, Hernandez C, Love MI, Chung HR*, et al.* ChIP-exo signal associated with DNA-binding motifs provides insight into the genomic binding of the glucocorticoid receptor and cooperating transcription factors. Genome Res **2015**;25(6):825-35 doi 10.1101/gr.185157.114.
21. Hu R, Lu C, Mostaghel EA, Yegnasubramanian S, Gurel M, Tannahill C*, et al.* Distinct transcriptional programs mediated by the ligand-dependent full-length androgen receptor and its splice variants in castration-resistant prostate cancer. Cancer Res **2012**;72(14):3457-62 doi 10.1158/0008-5472.CAN-11-3892.
22. Antony L, van der Schoor F, Dalrymple SL, Isaacs JT. Androgen receptor (AR) suppresses normal human prostate epithelial cell proliferation via AR/beta-catenin/TCF-4 complex inhibition of c-MYC transcription. Prostate **2014**;74(11):1118-31 doi 10.1002/pros.22828.
23. Zhang J, Gonit M, Salazar MD, Shatnawi A, Shemshedini L, Trumbly R*, et al.* C/EBPalpha redirects androgen receptor signaling through a unique bimodal interaction. Oncogene **2010**;29(5):723-38 doi 10.1038/onc.2009.373.
24. Watson PA, Arora VK, Sawyers CL. Emerging mechanisms of resistance to androgen receptor inhibitors in prostate cancer. Nat Rev Cancer **2015**;15(12):701-11 doi 10.1038/nrc4016.
25. Llukani E, Katz BF, Agalliu I, Lightfoot A, Yu SS, Kathrins M*, et al.* Low levels of serum testosterone in middle-aged men impact pathological features of prostate cancer. Prostate Int **2017**;5(1):17-23 doi 10.1016/j.prnil.2016.12.003.
26. Kim J, Davis JW, Klein EA, Magi-Galluzzi C, Lotan Y, Ward JF*, et al.* Tissue Effects in a Randomized Controlled Trial of Short-term Finasteride in Early Prostate Cancer. EBioMedicine **2016**;7:85-93 doi 10.1016/j.ebiom.2016.03.047.
27. Long MD, Campbell MJ. Pan-cancer analyses of the nuclear receptor superfamily. Nucl Receptor Res **2015**;2 doi 10.11131/2015/101182.
28. Cancer Genome Atlas Research N. Comprehensive molecular characterization of urothelial bladder carcinoma. Nature **2014**;507(7492):315-22 doi 10.1038/nature12965.
29. Cancer Genome Atlas N. Comprehensive molecular portraits of human breast tumours. Nature **2012**;490(7418):61-70 doi 10.1038/nature11412.
30. Cancer Genome Atlas N. Comprehensive molecular characterization of human colon and rectal cancer. Nature **2012**;487(7407):330-7 doi 10.1038/nature11252.
31. Cancer Genome Atlas N. Comprehensive genomic characterization of head and neck squamous cell carcinomas. Nature **2015**;517(7536):576-82 doi 10.1038/nature14129.

32. Ahn SM, Jang SJ, Shim JH, Kim D, Hong SM, Sung CO*, et al.* Genomic portrait of resectable hepatocellular carcinomas: implications of RB1 and FGF19 aberrations for patient stratification. Hepatology **2014**;60(6):1972-82 doi 10.1002/hep.27198.
33. Carithers LJ, Ardlie K, Barcus M, Branton PA, Britton A, Buia SA*, et al.* A Novel Approach to High-Quality Postmortem Tissue Procurement: The GTEx Project. Biopreserv Biobank **2015**;13(5):311-9 doi 10.1089/bio.2015.0032.
34. Cancer Genome Atlas Research N. The Molecular Taxonomy of Primary Prostate Cancer. Cell **2015**;163(4):1011-25 doi 10.1016/j.cell.2015.10.025.
35. Lehmann JM, Hoffmann B, Pfahl M. Genomic organization of the retinoic acid receptor gamma gene. Nucleic Acids Res **1991**;19(3):573-8.
36. Marques RB, Dits NF, Erkens-Schulze S, van Ijcken WF, van Weerden WM, Jenster G. Modulation of androgen receptor signaling in hormonal therapy-resistant prostate cancer cell lines. PLoS One **2011**;6(8):e23144 doi 10.1371/journal.pone.0023144.
37. Hua S, Kittler R, White KP. Genomic antagonism between retinoic acid and estrogen signaling in breast cancer. Cell **2009**;137(7):1259-71 doi 10.1016/j.cell.2009.04.043.
38. Kittler R, Zhou J, Hua S, Ma L, Liu Y, Pendleton E*, et al.* A comprehensive nuclear receptor network for breast cancer cells. Cell Rep **2013**;3(2):538-51 doi 10.1016/j.celrep.2013.01.004.
39. Sallari RC, Sinnot-Armstrong, N.A., French, J.D., Kron, K.J., Ho, J., Moore, J. H., Stambolic, V., Edwards, S. L., Lupien, M., Kellis, M.,. Convergence of dispersed regulatory mutations predicts driver genes in prostate cancer. BioRxiv **2017** doi doi: https://doi.org/10.1101/097451.
40. Murakawa Y, Yoshihara M, Kawaji H, Nishikawa M, Zayed H, Suzuki H*, et al.* Enhanced Identification of Transcriptional Enhancers Provides Mechanistic Insights into Diseases. Trends Genet **2016**;32(2):76-88 doi 10.1016/j.tig.2015.11.004.
41. Andersson R, Gebhard C, Miguel-Escalada I, Hoof I, Bornholdt J, Boyd M*, et al.* An atlas of active enhancers across human cell types and tissues. Nature **2014**;507(7493):455-61 doi 10.1038/nature12787.
42. Tan PY, Chang CW, Chng KR, Wansa KD, Sung WK, Cheung E. Integration of regulatory networks by NKX3-1 promotes androgen-dependent prostate cancer survival. Mol Cell Biol **2012**;32(2):399-414 doi 10.1128/MCB.05958-11.
43. Cicek MS, Liu X, Casey G, Witte JS. Role of androgen metabolism genes CYP1B1, PSA/KLK3, and CYP11alpha in prostate cancer risk and aggressiveness. Cancer Epidemiol Biomarkers Prev **2005**;14(9):2173-7 doi 10.1158/1055-9965.EPI-05-0215.
44. de Lau W, Peng WC, Gros P, Clevers H. The R-spondin/Lgr5/Rnf43 module: regulator of Wnt signal strength. Genes Dev **2014**;28(4):305-16 doi 10.1101/gad.235473.113.
45. Yu YP, Yu G, Tseng G, Cieply K, Nelson J, Defrances M*, et al.* Glutathione peroxidase 3, deleted or methylated in prostate cancer, suppresses prostate cancer growth and metastasis. Cancer Res **2007**;67(17):8043-50 doi 10.1158/0008-5472.CAN-07-0648.
46. He M, Vanaja DK, Karnes RJ, Young CY. Epigenetic regulation of Myc on retinoic acid receptor beta and PDLIM4 in RWPE1 cells. Prostate **2009**;69(15):1643-50 doi 10.1002/pros.21013.
47. Chen C, Dienhart JA, Bolton EC. Androgen-Sensitized Apoptosis of HPr-1AR Human Prostate Epithelial Cells. PLoS One **2016**;11(5):e0156145 doi 10.1371/journal.pone.0156145.
48. Dhiman VK, Attwood K, Campbell MJ, Smiraglia DJ. Hormone stimulation of androgen receptor mediates dynamic changes in DNA methylation patterns at regulatory elements. Oncotarget **2015**;6(40):42575-89 doi 10.18632/oncotarget.6471.
49. Dweep H, Sticht C, Pandey P, Gretz N. miRWalk--database: prediction of possible miRNA binding sites by "walking" the genes of three genomes. Journal of biomedical informatics **2011**;44(5):839-47 doi 10.1016/j.jbi.2011.05.002.

50. Kwabi-Addo B, Giri D, Schmidt K, Podsypanina K, Parsons R, Greenberg N*, et al.* Haploinsufficiency of the Pten tumor suppressor gene promotes prostate cancer progression. Proc Natl Acad Sci U S A **2001**;98(20):11563-8 doi 10.1073/pnas.201167798.
51. Foster BA, Gingrich JR, Kwon ED, Madias C, Greenberg NM. Characterization of prostatic epithelial cell lines derived from transgenic adenocarcinoma of the mouse prostate (TRAMP) model. Cancer Res **1997**;57(16):3325-30.
52. Ellwood-Yen K, Graeber TG, Wongvipat J, Iruela-Arispe ML, Zhang J, Matusik R*, et al.* Myc-driven murine prostate cancer shares molecular features with human prostate tumors. Cancer Cell **2003**;4(3):223-38.
53. Haflidadottir BS, Larne O, Martin M, Persson M, Edsjo A, Bjartell A*, et al.* Upregulation of miR-96 enhances cellular proliferation of prostate cancer cells through FOXO1. PLoS One **2013**;8(8):e72400 doi 10.1371/journal.pone.0072400.
54. Guttilla IK, White BA. Coordinate regulation of FOXO1 by miR-27a, miR-96, and miR-182 in breast cancer cells. J Biol Chem **2009**;284(35):23204-16 doi 10.1074/jbc.M109.031427.
55. Siu MK, Tsai YC, Chang YS, Yin JJ, Suau F, Chen WY*, et al.* Transforming growth factor-beta promotes prostate bone metastasis through induction of microRNA-96 and activation of the mTOR pathway. Oncogene **2015**;34(36):4767-76 doi 10.1038/onc.2014.414.
56. Tan SM, Lieberman J. Capture and Identification of miRNA Targets by Biotin Pulldown and RNA-seq. Methods Mol Biol **2016**;1358:211-28 doi 10.1007/978-1-4939-3067-8_13.
57. Jones HE, Eaton CL, Barrow D, Dutkowski C, Griffiths K. Response of cell growth and retinoic acid receptor expression to retinoic acid in neoplastic and non-neoplastic prostate cell lines. Prostate **1997**;30(3):174-82.
58. Guyot R, Vincent S, Bertin J, Samarut J, Ravel-Chapuis P. The transforming acidic coiled coil (TACC1) protein modulates the transcriptional activity of the nuclear receptors TR and RAR. BMC Mol Biol **2010**;11:3 doi 10.1186/1471-2199-11-3.
59. Luo Z, Gao X, Lin C, Smith ER, Marshall SA, Swanson SK*, et al.* Zic2 is an enhancer-binding factor required for embryonic stem cell specification. Mol Cell **2015**;57(4):685-94 doi 10.1016/j.molcel.2015.01.007.
60. Qiu JJ, Lu X, Zeisig BB, Ma Z, Cai X, Chen S*, et al.* Leukemic transformation by the APL fusion protein PRKAR1A-RAR{alpha} critically depends on recruitment of RXR{alpha}. Blood **2010**;115(3):643-52 doi 10.1182/blood-2009-07-232652.
61. Ozpolat B, Akar U, Zorrilla-Calancha I, Vivas-Mejia P, Acevedo-Alvarez M, Lopez-Berestein G. Death-associated protein 5 (DAP5/p97/NAT1) contributes to retinoic acid-induced granulocytic differentiation and arsenic trioxide-induced apoptosis in acute promyelocytic leukemia. Apoptosis **2008**;13(7):915-28 doi 10.1007/s10495-008-0222-9.
62. Hindley CJ, Condurat AL, Menon V, Thomas R, Azmitia LM, Davis JA*, et al.* The Hippo pathway member YAP enhances human neural crest cell fate and migration. Sci Rep **2016**;6:23208 doi 10.1038/srep23208.
63. Johannesson M, Stahlberg A, Ameri J, Sand FW, Norrman K, Semb H. FGF4 and retinoic acid direct differentiation of hESCs into PDX1-expressing foregut endoderm in a time- and concentration-dependent manner. PLoS One **2009**;4(3):e4794 doi 10.1371/journal.pone.0004794.
64. Liu P, Ramachandran S, Ali Seyed M, Scharer CD, Laycock N, Dalton WB*, et al.* Sex-determining region Y box 4 is a transforming oncogene in human prostate cancer cells. Cancer Res **2006**;66(8):4011-9 doi 10.1158/0008-5472.CAN-05-3055.
65. Lohnes D, Kastner P, Dierich A, Mark M, LeMeur M, Chambon P. Function of retinoic acid receptor gamma in the mouse. Cell **1993**;73(4):643-58.

66. Roadmap Epigenomics C, Kundaje A, Meuleman W, Ernst J, Bilenky M, Yen A*, et al.* Integrative analysis of 111 reference human epigenomes. Nature **2015**;518(7539):317-30 doi 10.1038/nature14248.
67. Simandi Z, Horvath A, Wright LC, Cuaranta-Monroy I, De Luca I, Karolyi K*, et al.* OCT4 Acts as an Integrator of Pluripotency and Signal-Induced Differentiation. Mol Cell **2016**;63(4):647-61 doi 10.1016/j.molcel.2016.06.039.
68. Chen CF, Goyette P, Lohnes D. RARgamma acts as a tumor suppressor in mouse keratinocytes. Oncogene **2004**;23(31):5350-9 doi 10.1038/sj.onc.1207682.
69. Kashyap V, Laursen KB, Brenet F, Viale AJ, Scandura JM, Gudas LJ. RARgamma is essential for retinoic acid induced chromatin remodeling and transcriptional activation in embryonic stem cells. J Cell Sci **2013**;126(Pt 4):999-1008 doi 10.1242/jcs.119701.
70. Su D, Gudas LJ. Gene expression profiling elucidates a specific role for RARgamma in the retinoic acid-induced differentiation of F9 teratocarcinoma stem cells. Biochem Pharmacol **2008**;75(5):1129-60 doi 10.1016/j.bcp.2007.11.006.
71. Seewaldt VL, Johnson BS, Parker MB, Collins SJ, Swisshelm K. Expression of retinoic acid receptor beta mediates retinoic acid-induced growth arrest and apoptosis in breast cancer cells. Cell growth & differentiation : the molecular biology journal of the American Association for Cancer Research **1995**;6(9):1077-88.
72. Itkonen HM, Brown M, Urbanucci A, Tredwell G, Ho Lau C, Barfeld S*, et al.* Lipid degradation promotes prostate cancer cell survival. Oncotarget **2017**;8(24):38264-75 doi 10.18632/oncotarget.16123.
73. Zhang S, Yu M, Liu C, Wang L, Hu Y, Bai Y*, et al.* MIR-34c regulates mouse embryonic stem cells differentiation into male germ-like cells through RARg. Cell biochemistry and function **2012**;30(8):623-32 doi 10.1002/cbf.2922.
74. Tsai YC, Chen WY, Siu MK, Tsai HY, Yin JJ, Huang J*, et al.* Epidermal growth factor receptor signaling promotes metastatic prostate cancer through microRNA-96-mediated downregulation of the tumor suppressor ETV6. Cancer Lett **2017**;384:1-8 doi 10.1016/j.canlet.2016.10.014.
75. Wang BD, Ceniccola K, Yang Q, Andrawis R, Patel V, Ji Y*, et al.* Identification and Functional Validation of Reciprocal microRNA-mRNA Pairings in African American Prostate Cancer Disparities. Clin Cancer Res **2015**;21(21):4970-84 doi 10.1158/1078-0432.CCR-14-1566.
76. Yu JJ, Wu YX, Zhao FJ, Xia SJ. miR-96 promotes cell proliferation and clonogenicity by down-regulating of FOXO1 in prostate cancer cells. Med Oncol **2014**;31(4):910 doi 10.1007/s12032-014-0910-y.
77. Kang SG, Ha YR, Kim SJ, Kang SH, Park HS, Lee JG*, et al.* Do microRNA 96, 145 and 221 expressions really aid in the prognosis of prostate carcinoma? Asian J Androl **2012**;14(5):752-7 doi 10.1038/aja.2012.68.
78. Cancer Genome Atlas Research Network. Electronic address scmo, Cancer Genome Atlas Research N. The Molecular Taxonomy of Primary Prostate Cancer. Cell **2015**;163(4):1011-25 doi 10.1016/j.cell.2015.10.025.
79. Mo W, Zhang J, Li X, Meng D, Gao Y, Yang S*, et al.* Identification of novel AR-targeted microRNAs mediating androgen signalling through critical pathways to regulate cell viability in prostate cancer. PLoS One **2013**;8(2):e56592 doi 10.1371/journal.pone.0056592.
80. Torrano V, Valcarcel-Jimenez L, Cortazar AR, Liu X, Urosevic J, Castillo-Martin M*, et al.* The metabolic co-regulator PGC1alpha suppresses prostate cancer metastasis. Nat Cell Biol **2016**;18(6):645-56 doi 10.1038/ncb3357.
81. Shiota M, Yokomizo A, Tada Y, Inokuchi J, Tatsugami K, Kuroiwa K*, et al.* Peroxisome proliferator-activated receptor gamma coactivator-1alpha interacts with the androgen receptor (AR) and

promotes prostate cancer cell growth by activating the AR. Mol Endocrinol **2010**;24(1):114-27 doi 10.1210/me.2009-0302.

82. Spahn M, Kneitz S, Scholz CJ, Stenger N, Rudiger T, Strobel P*, et al.* Expression of microRNA-221 is progressively reduced in aggressive prostate cancer and metastasis and predicts clinical recurrence. Int J Cancer **2010**;127(2):394-403 doi 10.1002/ijc.24715.
83. Gentleman RC, Carey VJ, Bates DM, Bolstad B, Dettling M, Dudoit S*, et al.* Bioconductor: open software development for computational biology and bioinformatics. Genome Biol **2004**;5(10):R80 doi 10.1186/gb-2004-5-10-r80.
84. Battaglia S, Maguire O, Thorne JL, Hornung LB, Doig CL, Liu S*, et al.* Elevated NCOR1 disrupts PPARalpha/gamma signaling in prostate cancer and forms a targetable epigenetic lesion. Carcinogenesis **2010**;31(9):1650-60 doi 10.1093/carcin/bgq086.
85. Chen Y, Lun AT, Smyth GK. From reads to genes to pathways: differential expression analysis of RNA-Seq experiments using Rsubread and the edgeR quasi-likelihood pipeline. F1000Res **2016**;5:1438 doi 10.12688/f1000research.8987.2.
86. Lun AT, Smyth GK. csaw: a Bioconductor package for differential binding analysis of ChIP-seq data using sliding windows. Nucleic Acids Res **2016**;44(5):e45 doi 10.1093/nar/gkv1191.
87. Ritchie ME, Phipson B, Wu D, Hu Y, Law CW, Shi W*, et al.* limma powers differential expression analyses for RNA-sequencing and microarray studies. Nucleic Acids Res **2015**;43(7):e47 doi 10.1093/nar/gkv007.
88. Love MI, Huber W, Anders S. Moderated estimation of fold change and dispersion for RNA-seq data with DESeq2. Genome Biol **2014**;15(12):550 doi 10.1186/s13059-014-0550-8.
89. Bolton EC, So AY, Chaivorapol C, Haqq CM, Li H, Yamamoto KR. Cell- and gene-specific regulation of primary target genes by the androgen receptor. Genes Dev **2007**;21(16):2005-17 doi 10.1101/gad.1564207.
90. Zhang D, Park D, Zhong Y, Lu Y, Rycaj K, Gong S*, et al.* Stem cell and neurogenic gene-expression profiles link prostate basal cells to aggressive prostate cancer. Nat Commun **2016**;7:10798 doi 10.1038/ncomms10798.
91. Decker KF, Zheng D, He Y, Bowman T, Edwards JR, Jia L. Persistent androgen receptor-mediated transcription in castration-resistant prostate cancer under androgen-deprived conditions. Nucleic Acids Res **2012**;40(21):10765-79 doi 10.1093/nar/gks888.
92. Chakravarty D, Sboner A, Nair SS, Giannopoulou E, Li R, Hennig S*, et al.* The oestrogen receptor alpha-regulated lncRNA NEAT1 is a critical modulator of prostate cancer. Nat Commun **2014**;5:5383 doi 10.1038/ncomms6383.

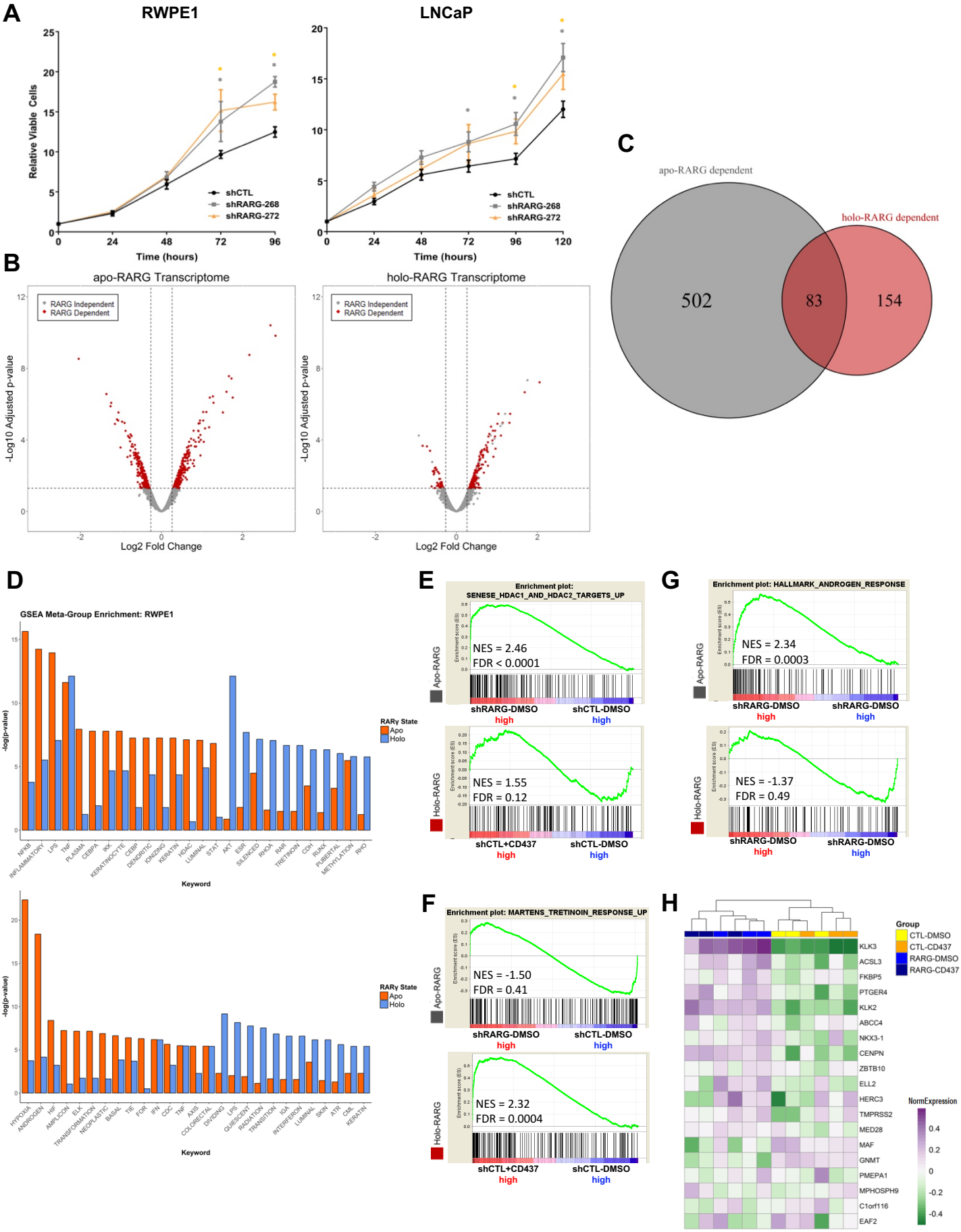
A
RWPE1
LNCaP
Relative Viable Cells
Time (hours)
shCTL
shRARG-268
shRARG-272
B
apo-RARG Transcriptome
holo-RARG Transcriptome
RARG Independent
RARG Dependent
-Log10 Adjusted p-value
Log2 Fold Change
C
apo-RARG dependent
holo-RARG dependent
502
83
154
D
GSEA Meta-Group Enrichment: RWPE1
-log(p-value)
RARγ State
Apo
Holo
Keyword
E
Enrichment plot: SENESE_HDAC1_AND_HDAC2_TARGETS_UP
Apo-RARG
NES = 2.46
FDR < 0.0001
shRARG-DMSO
high
shCTL-DMSO
high
Holo-RARG
NES = 1.55
FDR = 0.12
shCTL+CD437
high
shCTL-DMSO
high
G
Enrichment plot: HALLMARK_ANDROGEN_RESPONSE
Apo-RARG
NES = 2.34
FDR = 0.0003
shRARG-DMSO
high
shRARG-DMSO
high
Holo-RARG
NES = -1.37
FDR = 0.49
shRARG-DMSO
high
shRARG-DMSO
high
F
Enrichment plot: MARTENS_TRETINOIN_RESPONSE_UP
Apo-RARG
NES = -1.50
FDR = 0.41
shRARG-DMSO
high
shCTL-DMSO
high
Holo-RARG
NES = 2.32
FDR = 0.0004
shCTL+CD437
high
shCTL-DMSO
high
H
Group
CTL-DMSO
CTL-CD437
RARG-DMSO
RARG-CD437
KLK3
ACSL3
FKBP5
PTGER4
KLK2
ABCC4
NKX3-1
CENPN
ZBTB10
ELL2
HERC3
TMPRSS2
MED28
MAF
GNMT
PMEPA1
MPHOSPH9
C1orf116
EAF2
NormExpression

Figure 1

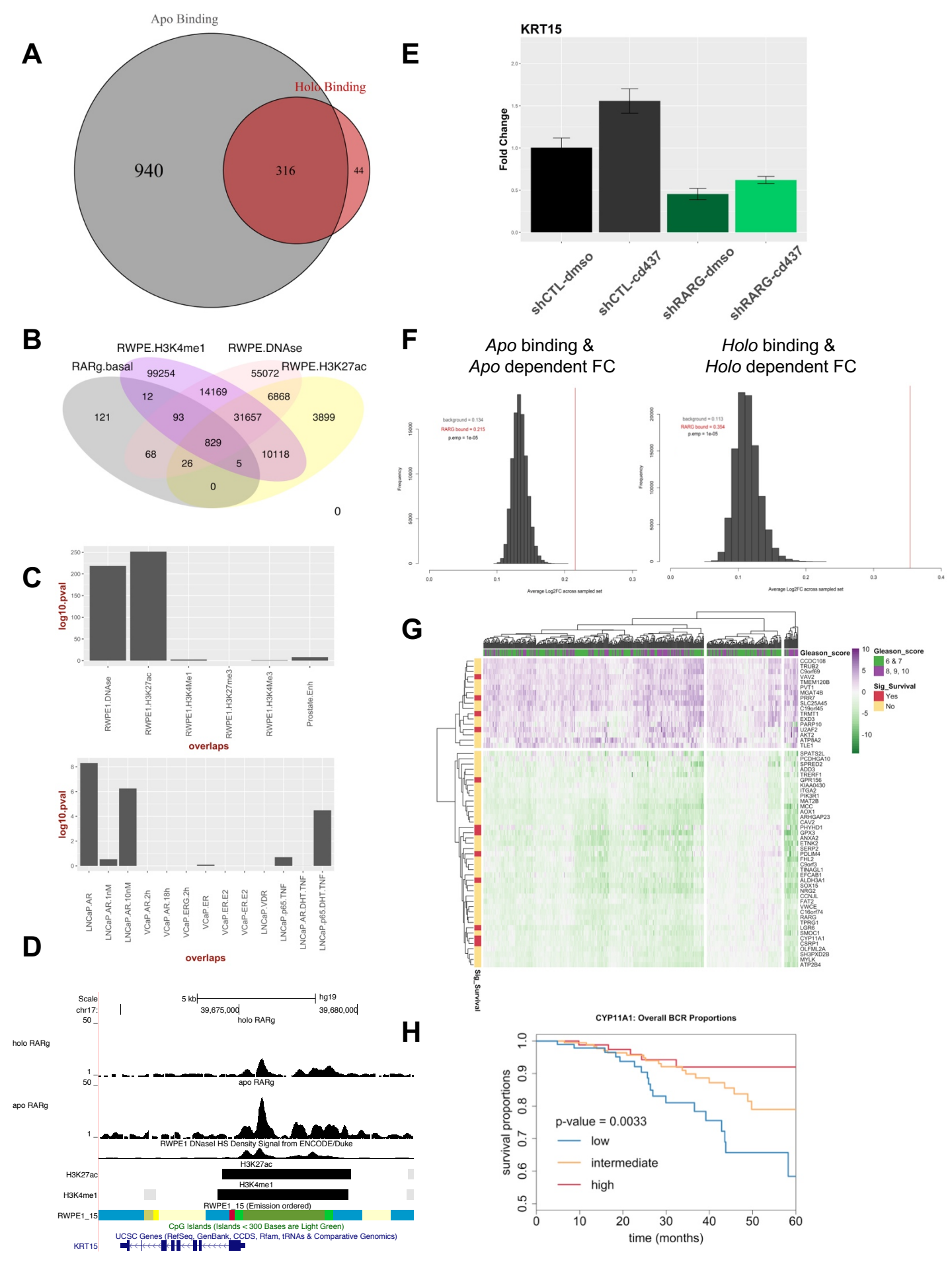
A
Apo Binding
Holo Binding
940
316
44
B
RWPE.H3K4me1
RWPE.DNAse
RARg.basal
RWPE.H3K27ac
99254
55072
14169
12
6868
121
93
31657
3899
829
68
26
5
10118
0
0
C
log10.pval
RWPE1.DNAse
RWPE1.H3K27ac
RWPE1.H3K4Me1
RWPE1.H3K27me3
RWPE1.H3K4Me3
Prostate.Enh
overlaps
log10.pval
LNCaP.AR
LNCaP.AR.1nM
LNCaP.AR.10nM
VCaP.AR.2h
VCaP.AR.18h
VCaP.ERG.2h
VCaP.ER
VCaP.ER.E2
VCaP-ER.E2
LNCaP.VDR
LNCaP.p65.TNF
LNCaP.AR.DHT.TNF-
LNCaP.p65.DHT.TNF-
overlaps
D
Scale
5 kb
hg19
chr17:
39,675,000
39,680,000
holo RARg
holo RARg
apo RARg
apo RARg
RWPE1 DNaseI HS Density Signal from ENCODE/Duke
H3K27ac
H3K27ac
H3K4me1
H3K4me1
RWPE1_15 (Emission ordered)
RWPE1_15
CpG Islands (Islands < 300 Bases are Light Green)
UCSC Genes (RefSeq, GenBank, CCDS, Rfam, tRNAs & Comparative Genomics)
KRT15
E
KRT15
Fold Change
shCTL-dmso
shCTL-cd437
shRARG-dmso
shRARG-cd437
F
Apo binding &
Apo dependent FC
Holo binding &
Holo dependent FC
background = 0.134
RARG bound = 0.215
p.emp = 1e-05
background = 0.113
RARG bound = 0.354
p.emp = 1e-05
Frequency
Average Log2FC across sampled set
G
Gleason_score
6 & 7
8, 9, 10
Sig_Survival
Yes
No
Sig_Survival
H
CYP11A1: Overall BCR Proportions
survival proportions
p-value = 0.0033
low
intermediate
high
time (months)

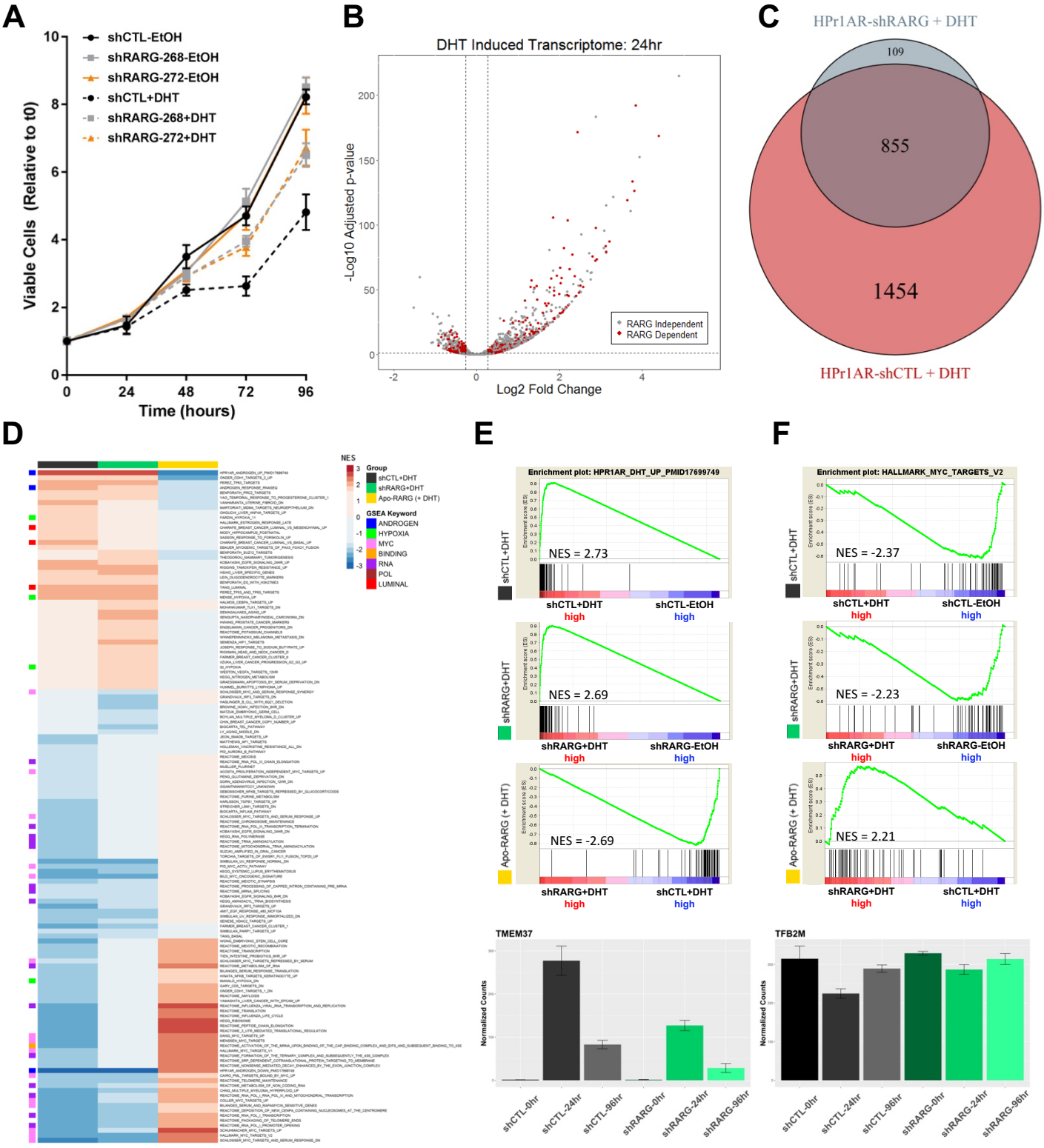
A
shCTL-EtOH
shRARG-268-EtOH
shRARG-272-EtOH
shCTL+DHT
shRARG-268+DHT
shRARG-272+DHT
Viable Cells (Relative to t0)
Time (hours)
B
DHT Induced Transcriptome: 24hr
-Log10 Adjusted p-value
Log2 Fold Change
RARG Independent
RARG Dependent
C
HPr1AR-shRARG + DHT
109
855
1454
HPr1AR-shCTL + DHT
D
NES
Group
shCTL+DHT
shRARG+DHT
Apo-RARG (+ DHT)
GSEA Keyword
ANDROGEN
HYPOXIA
MYC
BINDING
RNA
POL
LUMINAL
E
Enrichment plot: HPR1AR_DHT_UP_PMID17699749
NES = 2.73
NES = 2.69
NES = -2.69
shCTL+DHT high
shCTL-EtOH high
shRARG+DHT high
shRARG-EtOH high
F
Enrichment plot: HALLMARK_MYC_TARGETS_V2
NES = -2.37
NES = -2.23
NES = 2.21
TMEM37
TFB2M
Normalized Counts
shCTL-0hr
shCTL-24hr
shCTL-96hr
shRARG-0hr
shRARG-24hr
shRARG-96hr

Figure 3

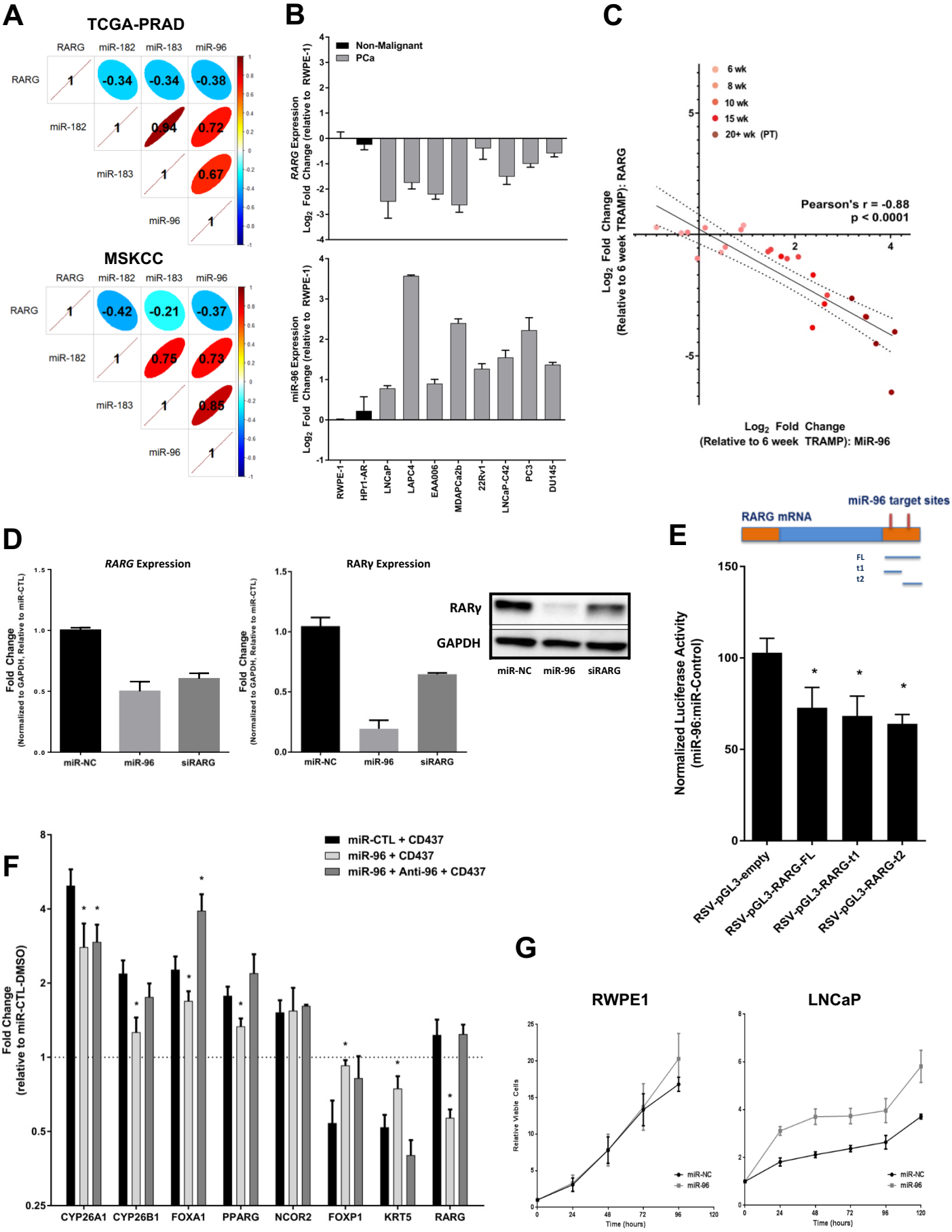
A
TCGA-PRAD
RARG
miR-182
miR-183
miR-96
1
-0.34
-0.34
-0.38
0.94
0.72
0.67
MSKCC
-0.42
-0.21
-0.37
0.75
0.73
0.85
B
Non-Malignant
PCa
RARG Expression
Log2 Fold Change (relative to RWPE-1)
miR-96 Expression
RWPE-1
HPr1-AR
LNCaP
LAPC4
EAA006
MDAPCa2b
22Rv1
LNCaP-C42
PC3
DU145
C
6 wk
8 wk
10 wk
15 wk
20+ wk (PT)
Pearson's r = -0.88
p < 0.0001
Log2 Fold Change
(Relative to 6 week TRAMP): RARG
Log2 Fold Change
(Relative to 6 week TRAMP): MiR-96
D
RARG Expression
Fold Change
(Normalized to GAPDH, Relative to miR-CTL)
miR-NC
miR-96
siRARG
RARγ Expression
RARγ
GAPDH
E
miR-96 target sites
RARG mRNA
FL
t1
t2
Normalized Luciferase Activity
(miR-96:miR-Control)
RSV-pGL3-empty
RSV-pGL3-RARG-FL
RSV-pGL3-RARG-t1
RSV-pGL3-RARG-t2
F
miR-CTL + CD437
miR-96 + CD437
miR-96 + Anti-96 + CD437
Fold Change
(relative to miR-CTL-DMSO)
CYP26A1
CYP26B1
FOXA1
PPARG
NCOR2
FOXP1
KRT5
RARG
G
RWPE1
LNCaP
Relative Viable Cells
Time (hours)
miR-NC
miR-96

Figure 4

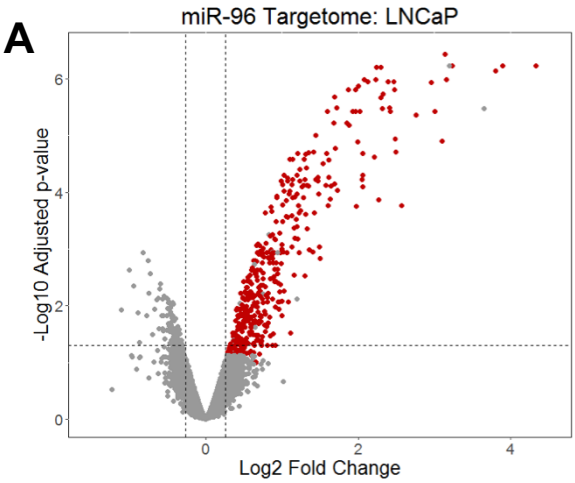
A
miR-96 Targetome: LNCaP
-Log10 Adjusted p-value
Log2 Fold Change

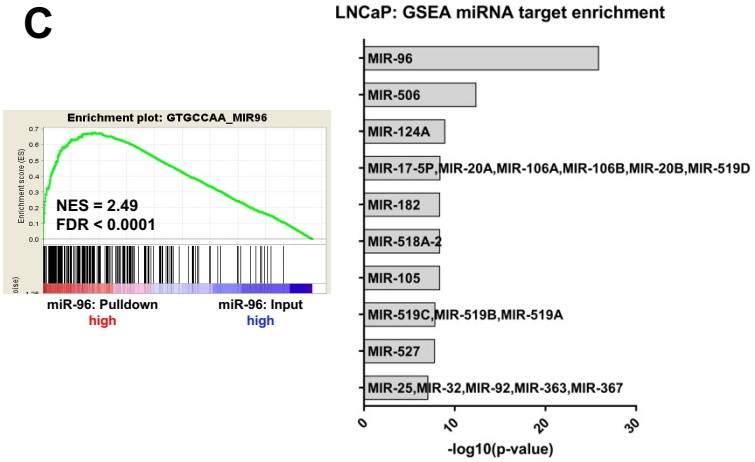
C
LNCaP: GSEA miRNA target enrichment
Enrichment plot: GTGCCAA_MIR96
NES = 2.49
FDR < 0.0001
miR-96: Pulldown
high
miR-96: Input
high
MIR-96
MIR-506
MIR-124A
MIR-17-5P,MIR-20A,MIR-106A,MIR-106B,MIR-20B,MIR-519D
MIR-182
MIR-518A-2
MIR-105
MIR-519C,MIR-519B,MIR-519A
MIR-527
MIR-25,MIR-32,MIR-92,MIR-363,MIR-367
-log10(p-value)

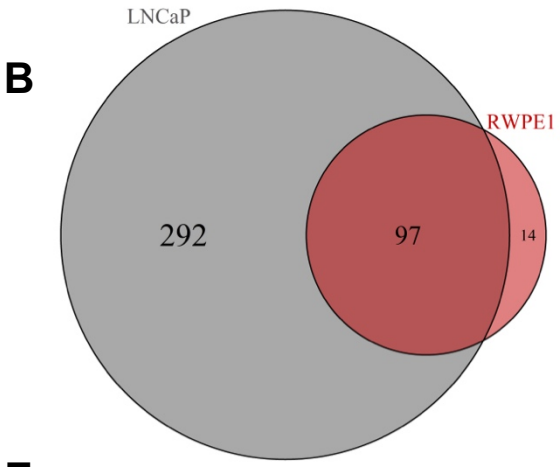
B
LNCaP
RWPE1
292
97
14

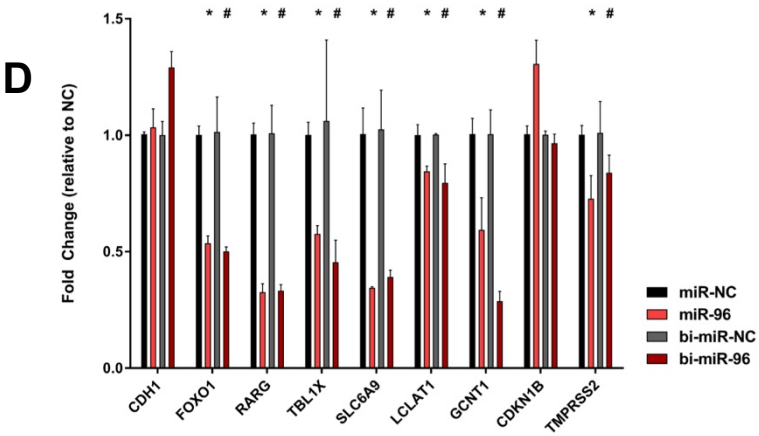
D
Fold Change (relative to NC)
CDH1
FOXO1
RARG
TBL1X
SLC6A9
LCLAT1
GCNT1
CDKN1B
TMPRSS2
miR-NC
miR-96
bi-miR-NC
bi-miR-96

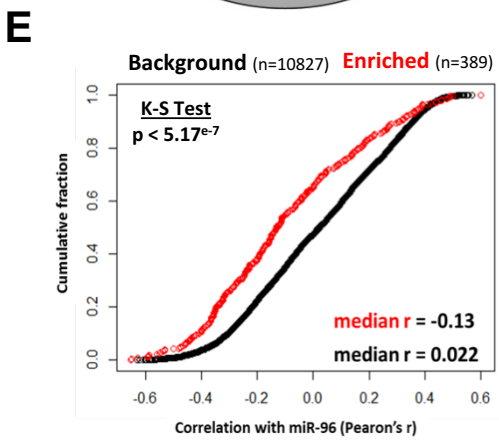
E
Background (n=10827)
Enriched (n=389)
K-S Test
p < 5.17e-7
median r = -0.13
median r = 0.022
Cumulative fraction
Correlation with miR-96 (Pearon's r)

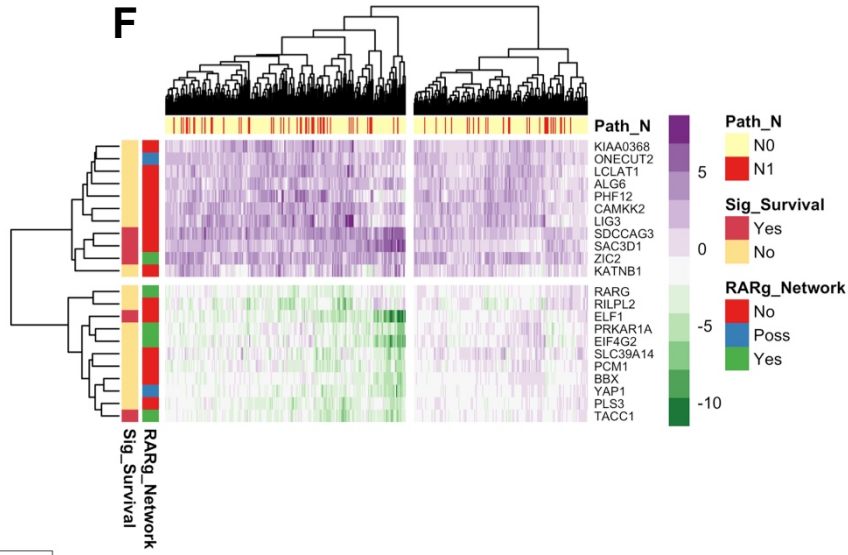
F
Path_N
KIAA0368
ONECUT2
LCLAT1
ALG6
PHF12
CAMKK2
LIG3
SDCCAG3
SAC3D1
ZIC2
KATNB1
RARG
RILPL2
ELF1
PRKAR1A
EIF4G2
SLC39A14
PCM1
BBX
YAP1
PLS3
TACC1
Path_N
N0
N1
Sig_Survival
Yes
No
RARg_Network
No
Poss
Yes
Sig_Survival
RARg_Network

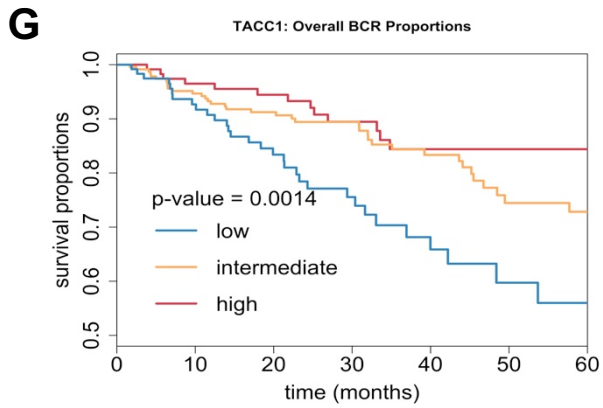
G
TACC1: Overall BCR Proportions
survival proportions
p-value = 0.0014
low
intermediate
high
time (months)

Figure 5

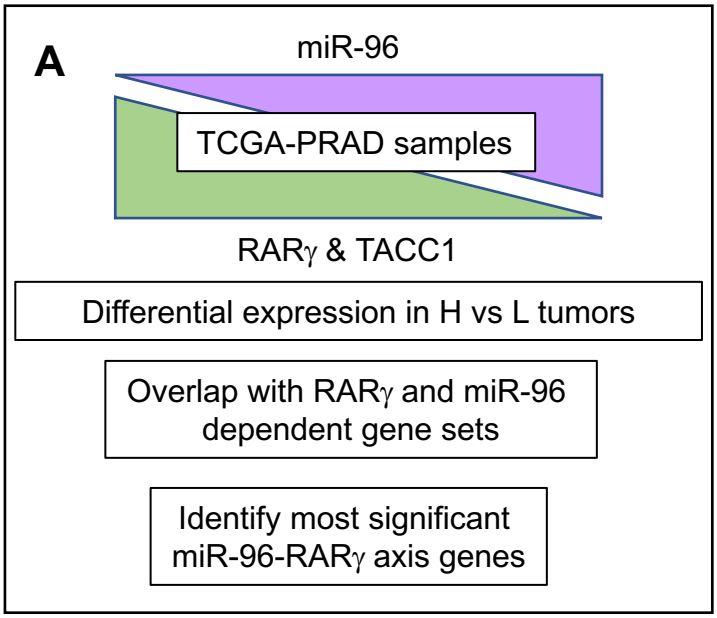
A
miR-96
TCGA-PRAD samples
RARγ & TACC1
Differential expression in H vs L tumors
Overlap with RARγ and miR-96 dependent gene sets
Identify most significant miR-96-RARγ axis genes

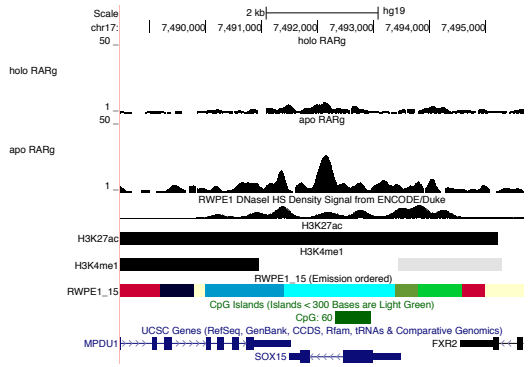
C
Scale
chr17:
2 kb
hg19
7,490,000
7,491,000
7,492,000
7,493,000
7,494,000
7,495,000
holo RARg
apo RARg
RWPE1 DNaseI HS Density Signal from ENCODE/Duke
H3K27ac
H3K4me1
RWPE1_15 (Emission ordered)
CpG Islands (Islands < 300 Bases are Light Green)
CpG: 60
UCSC Genes (RefSeq, GenBank, CCDS, Rfam, tRNAs & Comparative Genomics)
MPDU1
SOX15
FXR2

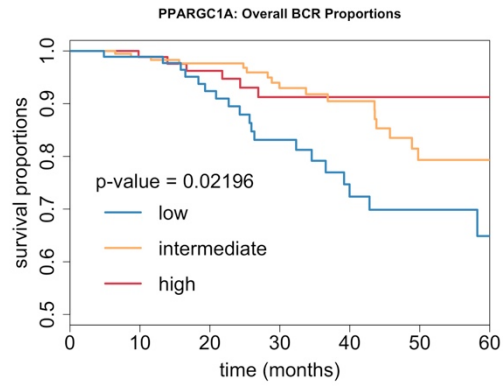
D
PPARGC1A: Overall BCR Proportions
survival proportions
time (months)
p-value = 0.02196
low
intermediate
high

B
Gleason_score
X_RFS_IND
SDCCAG3
SNHG3
EPHA10
RSAD1
SPATA18
ACOX2
PPARGC1A
MED21
HSPA4L
NR3C1
LOC255167
MBNL2
HCG11
NTF3
GPX3
RAB34
CTF1
PLP2
ETNK2
C1orf190
BEND5
RND2
SOX15
FBXO17
C7orf31
ROR2
PDPN
SNX7
PARP3
ANXA2P2
CDC42EP4
ST5
DOK4
EFNB1
FGFR2
GJA1
MCC
C5orf4
ANGPT1
TMLHE
JUB
IQCA1
PCP4L1
PAK7
NRG2
L3MBTL4
APOBEC3C
Liu_Down
Sig_Survival
RARg_AR
RARg_ChIP
Gleason_score
6 & 7
8, 9, 10
X_RFS_IND
No
Yes
Unk
Liu_Down
No
Yes
Sig_Survival
Yes
No
RARg_AR
No
Yes
RARg_ChIP
Yes
No